Chapter 3
High-Temperature Cuprate Superconductors and Later Discoveries

Abstract The discovery of superconductivity at 30 K in an oxygen deficient $La_4Ba_1Cu_5O_{5(3-y)}$ compound by Bednorz and Muller in 1986 marked a turning point in the history of superconductivity. The discovery at last lifted the despondency under which the superconductivity community was reeling since 1973 when a highest T_c = 23 K was recorded in sputtered Nb_3Ge films and the T_c went no further. Chu raised T_c of this compound to 40 K by applying pressure and Cava to 36 K after substituting Sr at the La site. A breakthrough came in early 1987 when Wu and Chu announced a record $T_c = 93$ K in $Y_1Ba_2Cu_3O_7$. T_c thus crossed the 77 K mark first time. Soon Maeda discovered superconductivity at 110 K in another cuprate of the type $Bi_2Sr_2Ca_2Cu_3O_{10}$ (Bi-2223 with 3 CuO_2 layers). These layered curates have large anisotropy. The superconductivity is strong in the a-b planes (CuO_2 layers) and weak along the *c*-axis. Critical parameters B_{c2} and J_c too are high in the *a–b* plane and low along *c*-direction. Both the materials, Bi-2223 and YBCO are produced commercially and used for selected applications. The new improved 2G YBCO wires are coated thin film conductors produced by employing sophisticated techniques and getting popularity among the community. Two more cuprates with still higher T_c and analogous to Bi-system were discovered. A $T_c = 125$ in $Tl_2Ca_2Ba_2Cu_3O_x$ (Tl-2223) and 135 K in $Hg_1Ba_2Ca_2Cu_3O_{6+\delta}$ (Hg-1223) were reported. These materials were, however, not pursued for commercial production because of the toxicity involved. Superconductivity was also discovered in MgB_2 at 39 K by Nagamatsu in 2001. MgB_2 behaves like a BCS superconductor but is characterized by two widely differing energy gaps, namely, 6.8 meV and 1.8 meV, two coherence lengths (13 and 51 nm) and two penetration depths (47.8 and 33.6 nm), respectively. This hinted at the presence of two species of electrons (σ bonding and π bonding) forming Cooper pairs. The material has low anisotropy of upper critical field $\left(\frac{B_{c2}^{ab}}{B_{c2}^{c}} = 1.1 - 1.7\right)$, high critical field, B_{c2} of up to 60 T and irreversible field B_{irr} up to 40 T. MgB_2 carries large self-field as well as in-field critical current at 20 K. One more surprise came when Hosano reported superconductivity in iron-based oxypnictides of the type LaFeAsO 1111 at 26 K. T_c in excess of 50 K were reported in Sm and Nd-based pnictides. The strategy adopted to enhance T_c has been to dope the insulating La_2O_2 layer suitably whereby a charge, electron/hole is transferred to the Fe_2As_2 conduction layer. Thus, a $T_c = 38$ K was reported in a K-doped $(Ba_{0.6}K_{0.4})Fe_2As_2$ 122 compound. Record high $T_c = 203$ K has been reported in sulphur hydride which has been found to be

R. G. Sharma, *Superconductivity*, Springer Series in Materials Science 214,
https://doi.org/10.1007/978-3-030-75672-7_3

a BCS superconductor. More recently, a $T_c = 288$ K (15 °C) has been reported in a C-S-H compound under a pressure of 267 GPa. This value of T_c is almost the room temperature.

3.1 Discovery of Superconductivity in La-Ba-Cu-O System ($T_c = 35$ K)

The search for superconductivity among the elements in the periodical table, in alloys and compounds continued unabated after the discovery of this fascinating phenomenon. Superconductivity was indeed discovered in a variety of families (listed in Table 3.1), but the T_c still remained confined to low value, necessitating the use of liquid helium for operation. The highest T_c was obtained in 1973–1974 in thin films of Nb_3Ge by Gavaler [1] and Tastardi et al. [2] by optimizing the deposition parameters. There was a lull for next 12 years until in 1986 all of a sudden, something very extraordinary happened. Two research scientists at IBM, Zűrich, namely, Bednorz and Muller discovered [3] superconductivity at 30 K in an oxide compound of the type $La_{5-x}Ba_xCu_5O_{5(3-y)}$. The compound was prepared by co-precipitation of the nitrates of La, Ba and Cu taken in appropriate ratios. This was followed by the solid-state reaction at 900 °C in a reduced atmosphere. Samples were finally prepared in the form of pellets sintered at 900 °C. The resistivity behaviour of these samples is shown in Fig. 3.1. Clearly, the resistivity drops with the fall of temperature nearly linearly, then rises logarithmically and then drops sharply by three orders of magnitude. The onset transition temperature is 30 K. Three phases were detected in the material: (i) a cubic phase dependent upon Ba composition, (ii) a superconducting phase $La_{1.8}Ba_{0.2}CuO_4$ and (iii) Perovskite layered phase of the type K_2NiF_4 with $a = 3.79$ Å and $c = 13.2$ Å. The resistivity was found to be changing with measuring sample current indicating that the superconductivity is granular in nature. The material turns out to be an O^{2-} deficient phase with mixed valence Cu constituents, namely, Jahn–Teller ions Cu^{2+} and non-Jahn—Teller ions Cu^{3+} resulting in a large λ (the electron–phonon coupling parameter) and large metallic conductivity. The ideal perovskite La_2CuO_4 structure is shown in Fig. 3.2 is orthorhombic at room temperature and becomes tetragonal at 500 K. Pure La_2CuO_4 is insulating and antiferromagnetic with a Neel temperature of 290 K. Ba and Sr substitute at La sites and the compound $La_{2-x}M_xCuO_4$ shows a T_c of 35 K at M = 0.15 and 0.2 for Ba and Sr, respectively. The doped material has a tetragonal structure at room temperature and turns orthorhombic at 180 K. It was not the first time that superconductivity was observed in oxides. As early as 1973, Johnston et al. [4] reported superconductivity in a Li-Ti-O system with a $T_c = 13.7$ K. The X-ray analysis showed the presence of three crystallographic phases. One phase with a spinel structure had the highest T_c with a comparatively low carrier concentration of $n = 2$–$4 \times 10^{21}/cm^3$. Soon after Sleight et al. [5] reported a $T_c = 13$ K in a mixed valence $BaPb_{1-x}Bi_xO_3$ system which also has a perovskite structure. Strong electron–phonon coupling was believed to be responsible for superconductivity. Prior to the discovery by Bednorz and Muller, scientists had almost given-up hopes of

Table 3.1 Different families of superconductors with corresponding T_c values (most values from [8], Courtesy R. P. Aloysius)

S. No.	Type of superconductor	Example	Max. T_c (K)
1.	Pure elements	Nb	9.2
2	Transition metal alloys	MoRe	12
3	Carbides	NbC	11
4	Nitrides	NbN	15
5	Amorphous superconductors	VGa	8.4
6	Nitrocarbides	$NbN_{0.7}C_{0.3}$	18
7	Laves phase (C-15 structure)	$CeRu_2$	6.1
8	Cheveral phase	$PbMo_6S_8$	12–14
9	A-15 (β-Tungsten)	Nb_3Sn-Nb_3Ge	18–23
10	Organic superconductors	$(TMTSF)_2PF_6$	1 (at 12 kbar)
11	Intercalated superconductors	$TaS_2(C_5H_5N)_{1/2}$	3.5
12	Heavy fermionic superconductors	UPt_3-$CeCoIn_5$	0.48–2.3
13	Magnetic superconductors	$ErRh_4B_4$	8.6
14	Semimetal superconductors	La_3Se_4	10
15	First oxide superconductors	$BiPb_{1-x}Bi_xO_3$	13 ($x = 0.25$)
16	K-doped Ba-Bi oxide, supercond.	$(Ba_{0.6}K_{0.4})BiO_3$	31.5
17	Boro-carbides	YNi_2B_2C	15
18	Rare earth cuperates	$YBa_2Cu_3O_{7-\delta}$	92
19	Lanthenate (discovery of high-T_c superconductor)	$La_{5-x}Ba_xCu_5O_{5(3-y)}$	35
20	Bismuth oxide superconductors (Bi-2223)	$Bi_{1.7}Pb_{0.4}Sr_{1.8}Ca_2Cu_{3.5}O_y$	110
21	Mercury oxide superconductors (Hg-1223)	$HgBa_2Ca_2Cu_3O_{8+\delta}$	155 (15 GPa)
22	Thallium oxide superconductors (Tl-2223)	$Tl_2Ca_2Ba_2Cu_3O_x$	125
23	Fullerides	Rb_2C_{60}	45
24	Magnesium diboride	MgB_2	39
25	Iron pnictides	$NdFeAsO_{0.82}F_{0.18}$	51
26	F-doped La-Fe-As compounds	$NdFeAsO_{0.82}F_{0.18}$	55 K
27	Iron chalcogenides	$Tl_{0.6}Rb_{0.4}Fe_{1.67}Se_2$	33

achieving high T_c in superconductors under the belief of the theoretical predictions made around the time. On the basis of the BCS theory even with highest values of the electron density of state and the electron–phonon coupling parameter, the T_c would not go beyond 30 K. What happened after the publication of the celebrated paper by Bednorz and Muller was something unprecedented and quite unexpected. Superconductivity was reported in oxide systems one after another with higher and

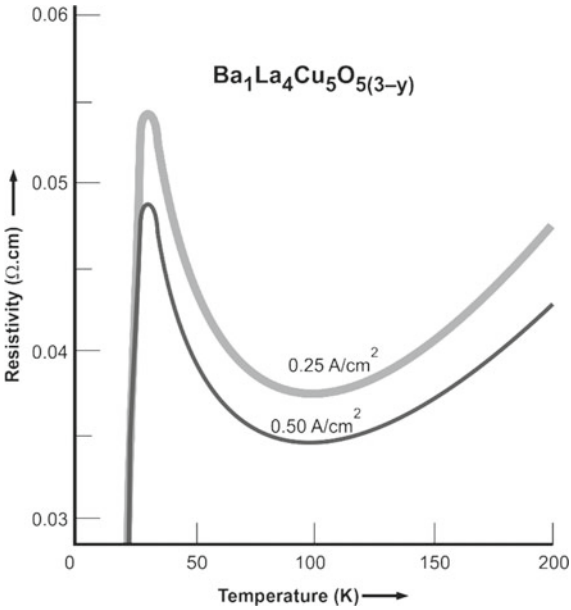

Fig. 3.1 Electrical resistivity plotted against temperature for the compound $La_4Ba_1Cu_5O_{5(3-y)}$. Superconducting transition occurs at ~ 30 K and the resistivity shows variation with measuring current [3]. With permission of Springer Science + Business Media

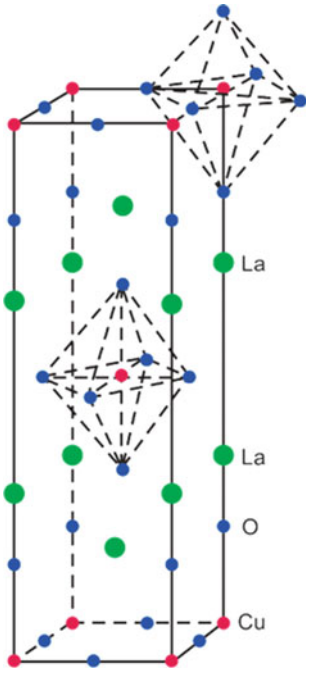

Fig. 3.2 Ideal La_2CuO_4 (K_2NiF_4) crystal structure. Superconductivity sets in with Ba/Sr substitution at the La site

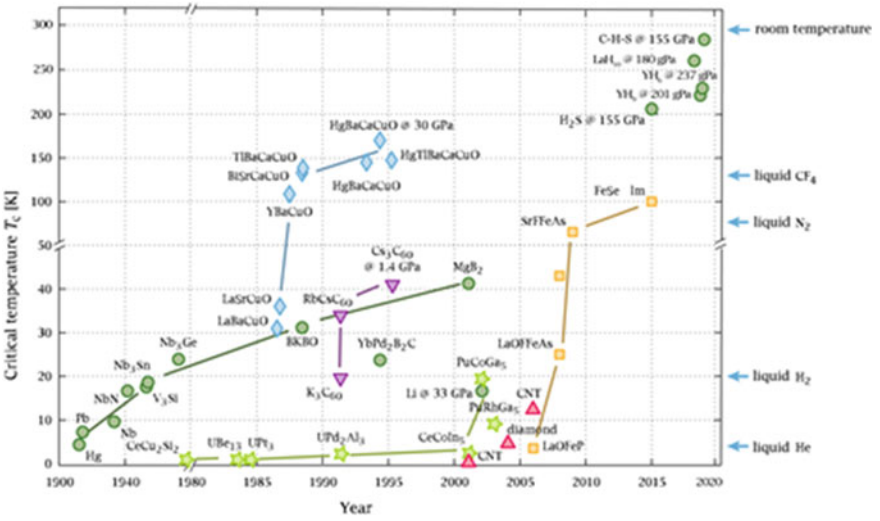

Fig. 3.3 Transition temperature (T_c) versus the year of discovery of the superconductor. The curve rose sharply in 1987 with the discovery of cuprates, in 2008 in iron based superconductors and in 2015 in sulphur hydride. Green circles are BCS superconductors, green stars heavy fermions, red triangles carbon allotropes, purple triangle buckminsterfullerenes, orange squares are iron–pnictogens and the blue diamonds are the cuprates. (Adapted from PJ Ray—CC BY-SA 4.0)

higher transition temperature, climbing well above the liquid nitrogen temperature (77 K) mark. Within a couple of years, T_c rose to as high as 150 K making the T_c/year graph rising almost exponentially (Fig. 3.3).

Chu et al. [6] at the University of Houston raised the T_c of the compound $(La_{0.85}Ba_{0.15})_2CuO_{4-y}$ from 36 K at ambient pressure to 40 K after applying a pressure of 13 K bar. Cava et al. [7], on the other hand, partially replaced La by Strontium replicating chemical pressure. The compound studied had the chemical composition $La_{1.8}Sr_{0.2}CuO_4$. Undoped La_2CuO_4 structure is slightly orthorhombic distortion of K_2NiF_4, all the copper ions are in Cu^{2+} state and no superconductivity is observed down to 4.2 K. Substitution of La by Sr stabilizes tetragonal undistorted K_2NiF_4 and oxidizes some Cu to Cu^{3+} state resulting in a mixed valence compound. The compound had been annealed in air as well as in oxygen [7]. Sample annealed in air revealed the presence of a mixture of a metallic phase, a semiconducting phase and a superconducting phase. Oxygen anneal on the other hand leads to a metallic and a superconducting phase. Oxygen anneal also improves the onset T_c from 36.5 to 38.5 K. Thus, Sr and oxygen both are important for the oxidizing condition. Oxygen pressure influences Cu^{3+}/Cu^{2+} valence ratio as well as charge compensation by O-vacancies.

The discovery of superconductivity by Bednorz and Műller in an oxide system opened the flood gate to the discovery of a larger family of oxide systems containing copper. Many superconductors containing Cu-O layers, now called cuprates with higher and higher T_c values rising far above the boiling temperature of nitrogen, 77 K

were discovered. This evoked great excitement among the scientific community of all shades who hoped that an engineering revolution will soon take place where the conventional superconductors used in large-scale applications will be replaced by these oxide superconductors. Although the hope of using these superconductors at 77 K for producing high magnetic fields has not been realized, yet selected cuprates have been produced commercially and are being increasingly used in a variety of power applications where high-current densities in presence of high magnetic field are not required. They have nevertheless been found suitable for high-field production, when operated below 65 K. A vast family of cuprate superconductors is tabulated along with their T_c values in Table 3.2.

Below we briefly discuss the discovery of important superconductors that surpassed the T_c of the previous superconductors.

3.2 The Y-Ba-Cu-O (YBCO) System—First Superconductor with T_c Above 77 K

A real breakthrough occurred in the history of superconductivity in March 1987 when Wu et al. [9] discovered superconductivity in a $Y_1Ba_2Cu_3O_{7-x}$ (or simply YBCO or also called just Y123) system at a T_c of 93 K making it possible first time to cool down a superconductor below its T_c using liquid nitrogen instead of liquid helium. Figure 3.4 shows the resistivity/temperature plots at different magnetic field reported by Wu et al. [9]. The superconducting phase was identified to be $Y_1Ba_2Cu_3O_7$ which is an oxygen deficient triplet perovskite unit cell of the type ABO_3. The triplet cell would have been $(Y_1Ba_2)Cu_3O_9$ but the superconducting phase is oxygen deficient that is, $Y_1Ba_2Cu_3O_7$ and has a $T_c = 93$ K. $Y_1Ba_2Cu_3O_7$ has an orthorhombic distorted structure and is shown in Fig. 3.5. Clearly, Cu ion has two distinct crystallographic and dissimilar sites Cu(1) and Cu(2). Cu(1) is surrounded by a squashed square planar O configuration in the *b*–*c* plane and linked to similar sites in a one dimension along the *b*-axis. Cu(2) site is 5 coordinated by a square pyramidal arrangement of O. The vertex of the pyramid is at O(4) site along the *c*-axis. The Y ion is at the centre of the two Cu-O sheets eight O-coordinated and Ba 10 O-coordinated. We thus find that Cu-O network is important for cuprates. Cu(1)–O(1) chains are crucial to superconductivity in this material. Cu(2)–O(2) and Cu(2)–O(3) do not seem to be so crucial for 90 K transition.

Cu(1)–O(4) bond is much stronger than Cu(1)–O(1), bond lengths being 1.85 Å and 1.943 Å, respectively. Oxygen vacancies occur on O(1) sites easily which brings down the transition temperature. At stoichiometric O_7, copper exists in divalent and trivalent state as per the expression below:

$$\text{At } O_7 \; Y_1Ba_2Cu_3O_7 \Rightarrow Y^{3+}Ba_2^{2+}Cu^{3+}(1)Cu_2^{2+}(2)O_7^{2-} \tag{3.1}$$

Table 3.2 Large variety of cuprate superconductors with their T_c values. 'n' represents the number of CuO_2 layers in the compound

S. No.	Compound	T_c (K)
1	$La_{1.85}(Ba/Sr)_{0.15}CuO_4$	35
2	$La_2CuO_{4+\delta}$	45
3	$La_{1.6}Sr_{0.4}CaCu_2O_{6+\delta}$	60
4	$Y_1Ba_2Cu_3O_7$	92
5	$Y_1Ba_2Cu_3O_8$	82
6	$TlBa_2Ca_{n-1}Cu_nO_{2n+3}$	120 ($n = 3$)
7	$TlBa_2Ca_{n-1}Cu_nO_{2n+4}$	127 ($n = 3$)
8	$Bi_2Sr_2Ca_{n-1}Cu_nO_{2n+4}$	110 ($n = 3$)
9	$HgBa_2Ca_{n-1}Cu_nO_{2n+2+\delta}$	134 ($n = 3$)
10	$CuBa_2Ca_{n-1}Cu_nO_7$	120
11	$Sr_2Ca_{n-1}Cu_nO_4$	90
12	$Pb_2Sr_2(Ca,Y,Nd)Cu_3O_8$	70
13	$Pb_2(Sr,La)_2Cu_2O_6$	32
14	$PbBaSrYCu_3O_8$	50
15	$(Pb,Cu)(Ba,Sr)_2(Y,Ca)Cu_2O_7$	53
16	$Pb_{0.5}Sr_{2.5}(Y.Ca)Cu_2O_7$	104
17	$(Pb,Cu)(Sr,La)_2CuO_5$	32
18	$(Nd,Ce)_2CuO_{4-\delta}$	24
19	$(Nd,Ce,Sr)CuO_{4-\delta}$	28
20	$(Pb,Cu,Eu,Ce)_2(Sr,Eu)_2Cu_2O_9$	25
21	$(EuCe)_2(Ba,Eu)_2Cu_3O_{10}$	43
22	$Bi_2Sr_2(Gd,Ce)_2Cu_2(CO_3)O_7$	34
23	$Tl_{0.5}Pb_{0.5}Sr_4Cu_2(CO_3)O_7$	70
24	$(BaSr)_2CuO_2(CO_3)$	40
25	$Sr_{4-x}Ba_xTlCu_2(CO_3)O_7$	62
26	$Tl_{0.5}Pb_{0.5}Sr_2Gd_{2-x}Ce_xCu_2O_{9-\delta}$	45
27	$NbSr_2(Gd,Ce)_2Cu_2O_y$	27
28	$Bi_2Sr_{6-x}Cu_3O_{10}(CO_3)_2$	40
29	$(Cu_{0.5}C_{0.5})Ba_2Ca_{n-1}Cu_nO_{2n+3}$	117 ($n = 4$)
30	$YCaBa_4Cu_5(NO_3)_{0.3}(CO_3)_{0.7}O_{11}$	82
31	$CuSr_{2-x}La_xYCu_2O_7$	60
32	$GaSr_2Ln_{1-x}Ca_xCu_2O_7$	73
33	$(C_{0.35}Cu_{0.65})Sr_2(Y_{0.73}Ce_{0.27})_2Cu_2O_x$	18
34	$Bi_4Sr_4CaCu_3O_{14+x}$	84

Data from [8], Courtesy R.P. Aloysius

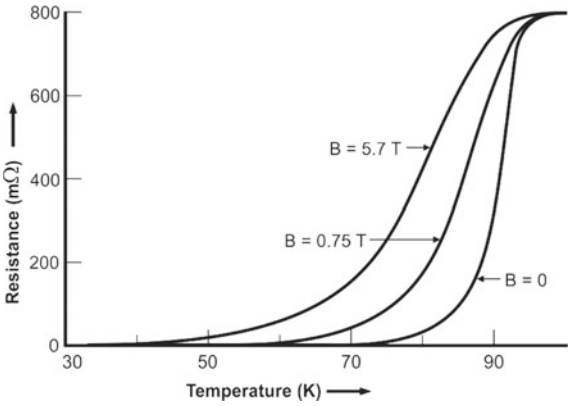

Fig. 3.4 Resistivity/temperature plot of Y-Ba-Cu-O at different magnetic fields by Wu et al. [9]. With permission from APS. http://journals.aps.org/prl/abstract/10.1103/PhysRevLett.58.908

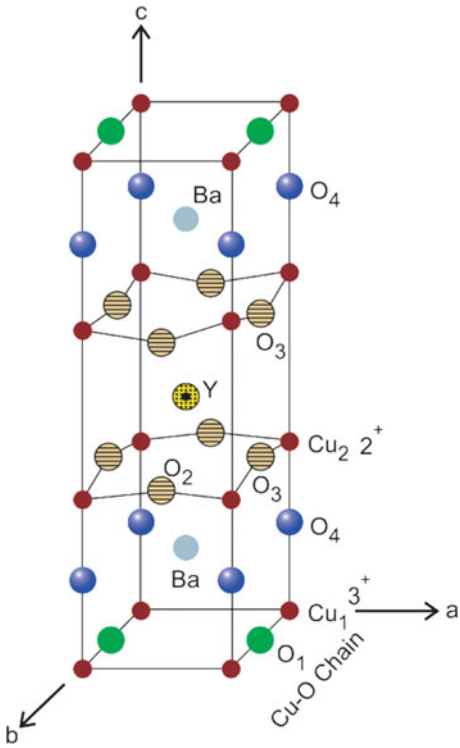

Fig. 3.5 Crystal structure of $Y_1Ba_2Cu_3O_7$. Notice two Cu-O sheets in the *a*–*b* plane sandwiching Y-atom and the Cu-O chains along the *b*-axis.

Oxygen depletion leads to change in structure from orthorhombic to tetragonal. T_c starts decreasing with oxygen loss and so does the oxidation state of Cu. As O-content decreases from 7 to 6.5, T_c decreases from 93 to 55 K and Cu(1) and Cu(2) are in divalent state. At O = 6.5, the material becomes semiconducting. In fact, there is a plateau in the T_c versus O-content curve at $O_{6.5}$. As O-content decreases further,

T_c decreases too and at O = 6, and the material turns in to an insulator. The oxidation state of Cu reduces to univalent. The oxidation states of Cu at O_6 and $O_{6.5}$ can be expressed like this:

$$\text{At } O_{6.5} \quad Y_1Ba_2Cu_3O_{6.5} = Y^{3+}Ba_2^{2+}cu^{2+}(1)Cu_2^{2+}(2)O_{6.5}^{2-} \tag{3.2}$$

$$\text{At } O_6 \quad Y_1Ba_2Cu_3O_6 = Y^{3+}Ba_2^{2+}Cu^{1+}(1)Cu_2^{2+}(2)O_6^{2-} \tag{3.3}$$

There is a striking correlation between the T_c and the oxidation state of Cu. T_c is found to be maximum when the oxidation state of Cu is $^{+}2.2$ which is found to correspond to O_7 stoichiometry. Both T_c and the copper oxidation state scales with the oxygen stoichiometry almost identically as seen from Fig. 3.6. T_c thus seems to be strongly dependent on the valence state of Cu which is controlled by the oxygen stoichiometry. One can explain this correlation between the valence state and T_c on the basis of the so-called charge transfer model. A detailed crystal structure of YBCO system, a repeat unit cell, is shown in Fig. 3.7. The CuO_2 planes sandwiching the Y-atom constitute the conduction layers. These double CuO_2 planes are separated by the so-called charge reservoir layers or the intercalating layers which consists of metal-oxygen layers of Cu, Ba and oxygen. Many cuprate superconductors have been discovered by manipulating the number of CuO_2 planes, metal atoms in the charge reservoir layer and crystal structure. Quite a few of these cuprates are tabulated along with their T_c values in Table 3.2. YBCO has two Cu-atoms per unit cell in the conduction layer and one Cu-atom in charge transfer layer forming Cu-O chains.

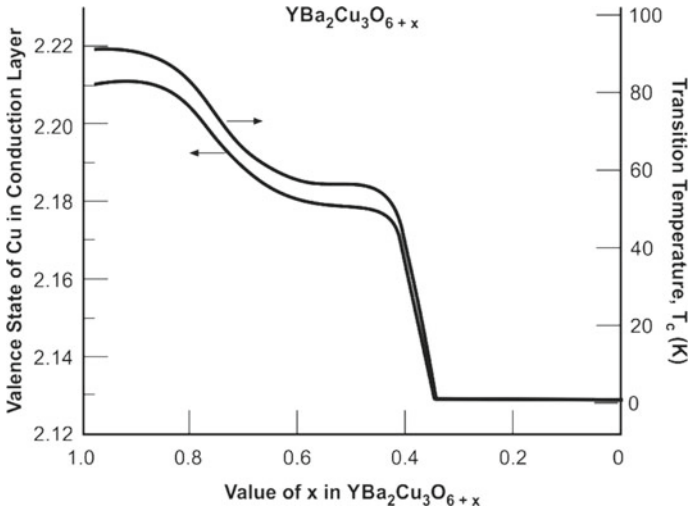

Fig. 3.6 T_c and the valence state of Cu in YBCO plotted against O-contents. T_c decreases as the oxygen content decreases from 7 to 6. Note the similarity in the two curves. Highest T_c occurs at $Cu^{+2.1}$. From my lecture notes, original data source could not be traced

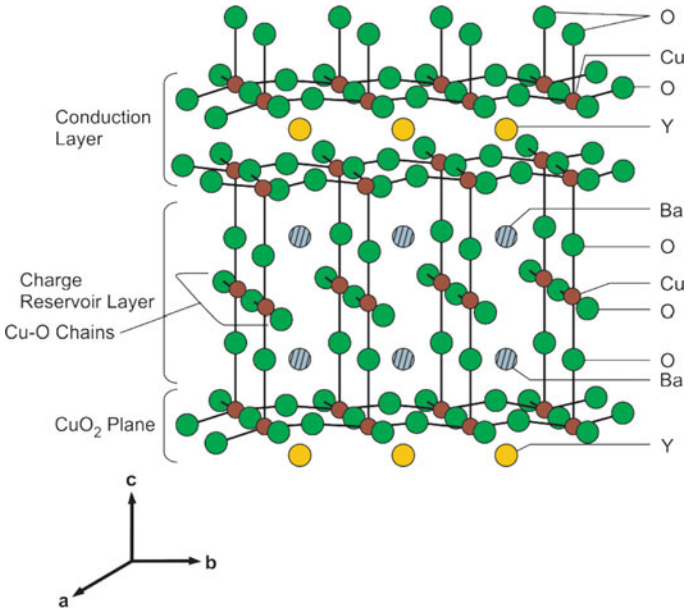

Fig. 3.7 Repeat unit cell structure of $Y_1Ba_2Cu_3O_{7-x}$. The CuO_2 planes on either side of Y-atom are the conduction layers and the Cu-O chains and the Ba-O planes constitute the charge reservoir layers

A reduction of O from 7 to 6 leads to equal distribution of O along the '*a*' and '*b*' axes and the structure changes from orthorhombic to tetragonal. The tetragonal phase is not superconducting. Holes are created in the conduction layers as the electrons are transferred to charge reservoir layers'. This changes the oxidation state of Cu to optimum value ($Cu^{+2.1}$) in the conduction layer causing the material to turn superconducting.

Even though YBCO remains to be the most studied and developed system, yet Y can be replaced by almost all the rare earth elements except Pr and Cs yielding this 123 compound with a $T_c = 90$ K. Even the magnetic material Gd yields Gd123 superconductor with $T_c = 90$ K.

3.2.1 Method of Synthesis of YBCO

The most popular technique for synthesizing Y123 is the standard technique of solid-state diffusion [10]. Appropriate quantities of Y_2O_3, $BaCO_3$ and CuO as per the formula unit $Y_1Ba_2Cu_3O_{7-x}$ are mixed thoroughly and ground in a pestle mortar. The fine powder so prepared is calcined at around 900 °C for about 20 h. This powder is finely crushed and calcined again. This process is repeated about three times when a homogenous mixture is obtained. The powder is now pressed in to the form of a pellet

or a bar and sintered at 920 °C for 20–25 h under flowing oxygen. Pieces of desired dimensions can now be cut from this pellet for different types of measurements. It is important to cool the sample slowly from the sintering temperature to have the stoichiometric oxygen (O_7) in the compound. Our experience shows around 60 °C/h. cooling rate is optimum [11]. Fast cooling changes the orthogonal phase in to the tetragonal phase and makes the material non-superconducting. Target pellets are also prepared for thin film deposition following this method. Adequate oxygen supply during the sintering process is essential to get oxygen stoichiometry to 7.0. This becomes rather difficult while supplying oxygen to Ag-clad wires. The author has used successfully an addition of HgO to the bulk YBCO before calcination which provides an internal source of oxygen [12–14]. A perfect O_7 stoichiometry has been obtained using this technique.

3.2.2 Some Peculiar Properties of YBCO

These cuprate superconductors are highly anisotropic materials and have widely different characteristic parameters and properties in the *a–b* plane and along the *c*-axis. Among the family of cuprates YBCO is, however, the least anisotropic. A well-oxygenated stoichiometric YBCO superconductor, for example, has the following typical parameters (Table 3.3).

Another peculiar property observed in these cuprates was the linear variation of the normal state resistivity with temperature down to T_c. This linear ρ–T behaviour in these compounds cannot be explained on the basis of electron–phonon interaction since the mean free path (~ 100–200 Å) is much greater than the lattice parameter (~ 3.8 Å).

Table 3.3 Typical parameters of a stoichiometric $Y_1Ba_2Cu_3O_7$ in the *a–b* plane and along the *c*-axis

Parameter	$Y_1Ba_2Cu_3O_7$
Critical temperature, T_c (K)	93 K
Lattice parameters	$a = 3.8591$ Å $b = 3.9195$ Å $c = 11.8431$ Å
Coherence length (0 K)	$\xi_{ab}(0) = 15$ Å $\xi_c(0) = 3$ Å
London penetration depth	$\lambda_{ab}(0) = 1400$ Å $\lambda_c(0) = 7000$ Å
Normal state resistivity	$\rho_{ab} = 0.5$ mΩ cm and metallic $\rho_c = 20$ mΩ cm and semiconducting

3.2.3 YBCO Wires and Tapes

High hopes were generated, first time, to use this material for high-field superconducting magnets and operate them at 77 K but the results were disappointing. The critical current in bulk YBCO superconductor drops down sharply with the application of magnetic field for a variety of reasons. One important reason is that these materials happen to be granular [10, 15] with grain boundaries which are weakly superconducting or even insulating. High critical current densities have however been reported in epitaxially grown YBCO films [16] and in YBCO single crystals [17]. This resulted in high expectation of developing this material with high critical current densities needed for high-field applications. The critical current within the grain has been found to be quite high ~ 10^6 A cm^{-2} at 77 K. After a few years of intensive research, the focus of R&D activity shifted from research laboratories to industry for their commercial production. American Superconductors, Furukawa, SuperPower and Sumitomo are some leading companies marketing HTS wires, tapes and current leads. 2G YBCO or rather 2G REBCO-coated conductors are increasingly used for power devices like fault current limiter (FCL), transformer and rotating machine. More recently, ingenious methods have been developed to produce REBCO cables capable of carrying tens of kA current. Full details of the fabrication techniques employed to produce these wires and cables will be discussed in Chap. 6 titled 'Practical Cuprate Superconductors'.

3.3 The Bi-Sr-Ca-Cu-O (BSCCO) System

Soon after the discovery of superconductivity in YBCO system at 93 K, Maeda et al. [18] reported superconductivity above 100 K in a Bi-Sr-Ca-Cu-O system, first high-T_c material without a rare earth element. Figure 3.8 shows the redrawn version of the original curve of the resistance versus temperature behaviour of this compound which happens to be a multiphase superconductor. This was the first observation made by Maeda's group on 24 December 1987. An onset of superconducting transition was observed at 114 K with a tendency to go to zero resistivity at 105 K. A second transition is observed showing zero resistivity at 80 K. Their initial attempts to isolate the high-T_c phase failed and they announced the discovery on 21 January 1988. Takano et al. [19], however, succeeded in stabilizing the high-T_c phase (= 110 K) through the partial substitution of Bi by Pb. Further studies established the coexistence of three distinct crystallographic phases, namely the $Bi(Pb)_2Sr_2Ca_2Cu_3O_x$ phase, $Bi_2Sr_2Ca_1Cu_2O_y$ phase and the $Bi_2Sr_2CuO_z$ or simply referred to as Bi-2223, Bi-2212 and Bi-2201 phases with T_c values of 110 K, 80 K and 10 K, respectively. In our laboratory, we have been obtaining phase pure Bi-2223 material by solid-state and also by solution technique with a T_c of 110 K. Best results have been obtained on nominal composition like $Bi_{1.6}Pb_{0.4}Sr_2Ca_{2.2}Cu_{3.5}O_y$ [20] and $Bi_{1.7}Pb_{0.4}Sr_{1.8}Ca_2Cu_{3.5}O_y$ [21] which are rich in Ca and Cu and deficient in

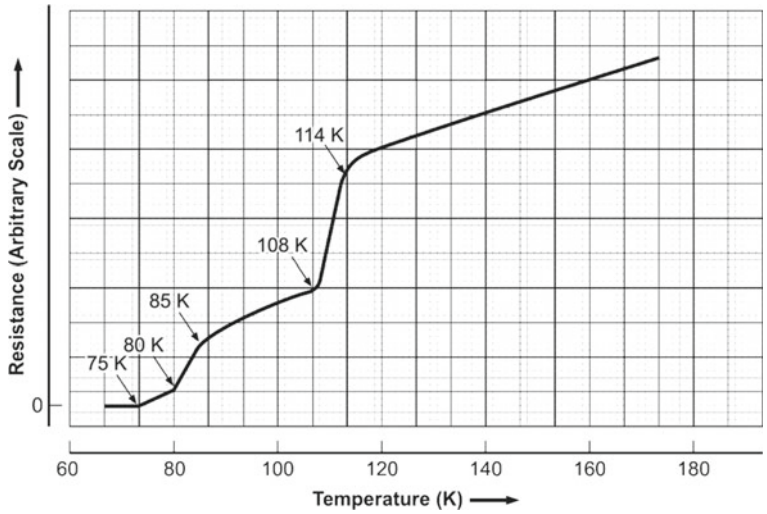

Fig. 3.8 Replicated original resistance versus temperature plot of Bi-Sr-Ca-Cu-O by Maeda et al. The curve shows multiple superconducting transitions at 114, 108 and 85 K [18]

Sr. These Bi-cuprates have orthorhombic structure and have Cu-O layers separated by Sr-O and Ca-O layers and two double Bi-O layers at the two ends of the unit cell. As seen from Fig. 3.9, the *c*-axis increases with the number of Cu-O layers. The *c*-axis is 24.6 Å for the 2201 phase, 30.89 Å for 2212 phase and 37.1 Å for the 2223 phase. There is one Cu-O layer in the 2201 phase, two Cu-O layers in 2212 phase and three Cu-O layers in the 2223 phase. It appears that T_c goes up as the number of Cu-O layers increase. T_c has however been found decreasing if the number of layers increases beyond three. Crystals of Bi-cuprates have mica like morphology. The 80 K Bi-2212 compound show modulation in the ab plane structure with 4b periodicity. The modulation is related to oxygen content and the Bi-O layers but does not play role in superconductivity. Inter-growth of the phases is a problem in the synthesis of Bi-compounds. Sometimes, this intergrowth has been found [21, 22] to provide effective flux pinning enhancing critical current density, J_c in Bi-2223 system.

3.3.1 Bi-2223 Wires and Tapes

Until the arrival of 2G, YBCO-coated tape conductors, Bi-2223 was the only material which has been commercially produced and used in applications like magnets, current leads high-gradient magnetic separators, fault current limiters and the likes. Bi-2223 had been the favourite high-T_c material for manufacturing because one needs to use a simple PIT technique followed by mechanical drawing, rolling and re-bundling

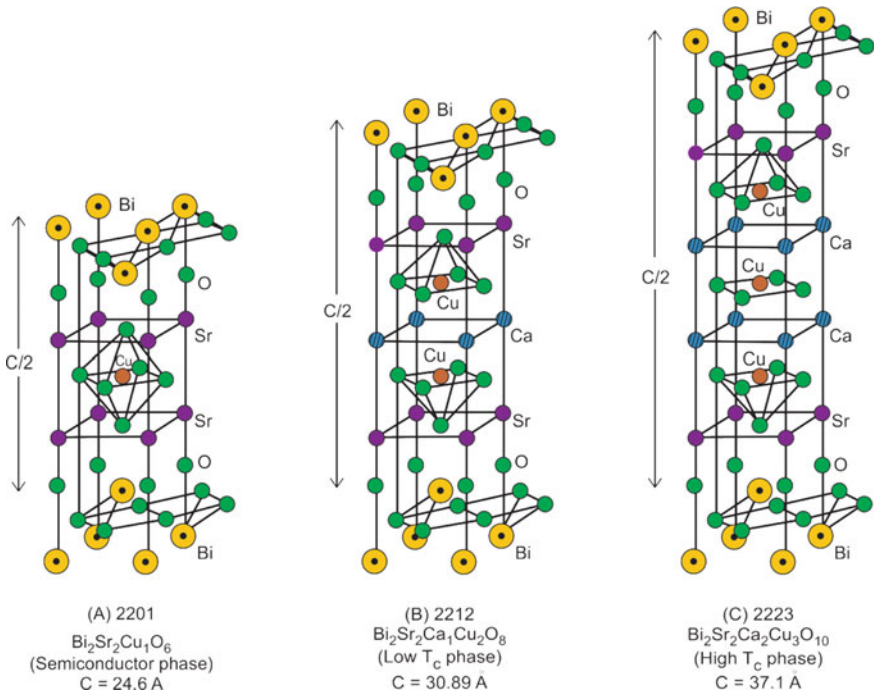

Fig. 3.9 Unit cells of the three Bi-compounds with compositions 2201, 2212 and 2223 having one, two and three Cu-O layers and increasing *c*-axis value, respectively

with intermediate heat treatments. Typical cross section of a circular wire and a rectangular tape with multifilaments are shown in Fig. 3.10. Another more subtle reason is that the *c*-axis grain alignment can easily be achieved when shaped in to the form of tapes. Grain alignment is achieved during the rolling process when compressive stress forces the plate-like Bi-2223 grains to align parallel to the tape surface. Weak link problem is thus minimized in this material. Bi-2212 on the other hand needs heat treatment of the partially melted material followed by solidification after the tape forming to get the grain alignment. NRIM (now NIMS) together with

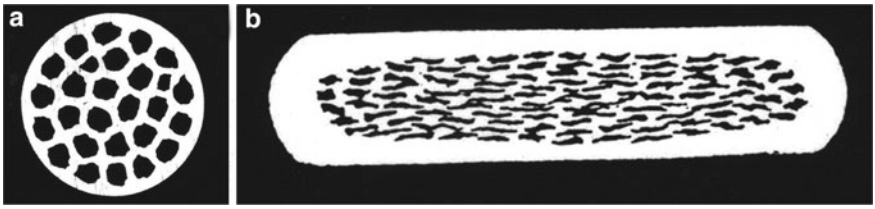

Fig. 3.10 Cross section of the multifilamentary Ag/B(P)SCCO wires and tapes [8]. *Courtesy* R. P. Aloysius

Asahi Glass and Hitachi Cable Group in Japan had produced a field of 21.8 T at 1.8 K by using a Bi-2212 coil [23] as the innermost insert. A background field of 18 T was provided by a combination of Nb-Ti and Nb_3Sn coils. The tapes were fabricated following the doctor-blade technique. More recently, round wires of Bi-2212 have been produced with high J_c by eliminating bubble formation in the grains through over-pressure heat treatment. This will be discussed in detail in Chap. 6.

The problem with high-T_c material is that the critical current density, J_c in these materials drops rather sharply in increased magnetic field when operated at high temperature, 77 K. This is primarily due to the weak pinning at these temperatures and the large anisotropy of J_c. Both are caused by the 2D nature of the structure of BSCCO system. Weakly superconducting or non-superconducting oxide layers separate the CuO_2 layers where the superconductivity resides. When a magnetic field is applied parallel to the layers (along the ab plane), vortices pass through the weakly superconducting layers (charge transfer layers), but CuO_2 layers prevent the vortex movement in the perpendicular direction. This is the new type of pinning force called 'intrinsic pinning' [24]. BSCCO tapes in parallel field configuration can thus be used even at 77 K and still carry significant current. In field parallel to *c*-axis, the vortex is divided into segments by non-superconducting layers because of extremely small coherence length along this axis. This segment is referred to as 'pancake vortex' [25] and is confined within the CuO_2 layer and free to move because it is not strongly connected with the vortex in the next layer. In our initial studies on MF Ag/BSCCO tapes [21], we found a variety of impurity induced defects which probably served good pinning centres in a low purity commercial (CuO 99%) grade material tapes. Figure 3.11a shows dislocation network in a (001) basal plane in a Ag/BSCCO-2223 tape with a core thickness of 140 μm. The same tape is further rolled to small thickness where the core thickness is reduced to 7 μm. As shown in Fig. 3.11b, the

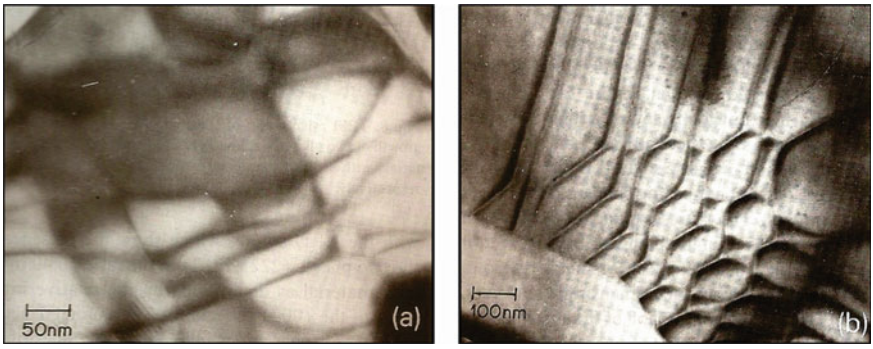

Fig. 3.11 Transmission electron micrographs of the core material of a Ag/BSCCO-2223 tape prepared using commercial grade oxides and carbonates. **a** is a tape with 140 μm thick core and shows dislocation network in (001) basal plane. **b** is the same tape rolled down to a core thickness of 7 μm and re-sintered. The density of dislocation increases in (b) sample. The dislocation network corresponds to the low-angle twist grain boundaries. J_c too increases [21]. With permission from Elsevier

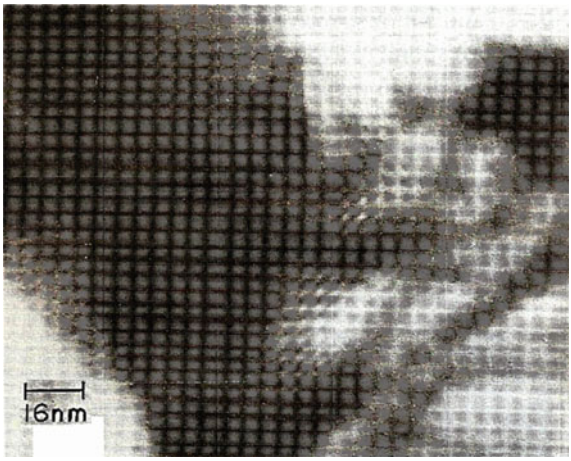

Fig. 3.12 TEM micrograph of (b) sample of Ag/BSCCO-2223 tape, rolled to fine size (7 μm core) and re-sintered, which shows the intergrowth of low T_c (2212) and high-T_c (2223) phases [21]. With permission from Elsevier

dislocation density increases and improves the flux pinning. The dislocation network corresponds to the low-angle grain boundaries. The J_c value of the 7 μm (b) sample is 6.14×10^3 A m^{-2} (77 K, self-field) and 1.49×10^5 A cm^{-2} (4.2 K, self-field). Yet another type of defect structure observed in the (b) sample is the inter-growth of the two phases, viz.; the low T_c (2212) and the high-T_c (2223) phase with a *c*-axis parameters of 30.89 Å and 37.1 Å, respectively. The J_c value after the rolling and re-sintering process is found to increase substantially. The commercial grade CuO (99 %) was found to have 60 ppm Fe which preferentially occupies the Cu(II) square pyramidal site as revealed by Mössbauer studies. This results in stacking faults and the intergrowth of the 2212 and 2223 phases (Fig. 3.12). These defects may be responsible for effective flux pinning and the higher J_c, as observed experimentally.

Among several manufacturers of the Ag/BSCCO wire, American Superconductors (AMSC) of USA and Sumitomo Electric Company (SEC) of Japan were the main players supplying this material for different applications. SEC of Japan had been marketing Ag-matrix clad BSCCO wires in long lengths under the code name DI-BSCCO wires [26]. AMSC mainly supplied two types of wires. One code named 1G-HSP HTS (high-strength plus HTS wire) meant for applications where high mechanical strength was required. This wire had BSCCO-based multifilaments (MF) and was encased in a Ag-alloy matrix with a SS lamination. We will discuss the cuprate wires and cables and their present status in Chap. 6 on 'Cuprate Practical Superconductors'.

3.3.2 First Generation (1G)-BSCCO Current Leads

One most popular use of BSCCO superconductor had been in current leads employed in superconducting magnets both bath-cooled and conduction-cooled. The BSCCO

Fig. 3.13 Bulk and encased current leads marketed by M/S 'Can Superconductors' and used in author's lab (IUAC New Delhi)

current leads capable of transporting current in excess of 3000 A have been commercially marketed for decades now. 'Can Superconductors' of Czech Republic, American Superconductors of USA and Bruker Energy & Supercon Technologies are some of the suppliers of these current leads. Current leads are generally used to transport current from 77 K thermal shield to magnet maintained at ~ 4 K with no Joule heating. Moreover, the thermal conduction through the leads too is poor which makes the magnet system energy efficient. Current carrying capacity almost doubles if the higher temperature end is kept at around 64 K instead of 77 K. Typically, a current lead with $I_c = 1500$ A between 77 and 4 K has a conductive heat leak of 0.6 W, whereas if used between 64 and 4 K the heat leak reduces to only 0.4 W. Current leads can be bulk tube type or encased for protection (Fig. 3.13).

Copper studs or copper braids are provided for jointing/soldering purpose. Figure 3.14 is a 100 A pair of BSCCO-2223 current leads developed [8] by the NIIST, Thiruvananthapuram. The development of BSCCO current leads made it possible to build cryo-free superconducting magnets, which found popularity in low temperature laboratories in last three decades. The reduction in heat generation in the current leads had been so significant that a closed-cycle refrigerator (CCR) with a cooling capacity of 1.5 W can cool a medium size magnet to ~ 3 K in a reasonable time of few hours. In Chap. 9, we will discuss the construction of a cryo-free magnet with a special reference to a 6 T room temperature bore magnet built in author's laboratory using a 1.5 W CCR of Sumitomo make many years ago.

Fig. 3.14 Pair of 100 A, BSCCO-2223 current leads developed by NIIST, Thiruvananthapuram. Leads with higher current rating available [8]. *Courtesy* R. P. Aloysius

3.4 The Tl-Ba-Ca-Cu-O System

The race to discover still higher T_c superconductors continued and yet one more cuprate superconductor of the type Tl-Ba-Ca-Cu-O with T_c of greater than 90 K was discovered by Sheng and Hermann [27] in 1988 itself. The zero resistivity in this compound was obtained at 81 K. Soon a T_c of 120 K was reported by the same authors [28] in a compound $Tl_{1.86}CaBaCu_3O_{7.5+y}$. This was the highest T_c cuprate without a rare earth constituent. Since Tl_2O_3, the ingredient of the compound has a low melting point of 717 °C and starts decomposing at 100 °C, and the preparation method for this compound is different. Sheng and Hermann have followed a 'short high temperature and quenching technique'. Appropriate amounts of $BaCO_3$ and CuO were mixed, ground and heated to 925 °C for > 24 h in air with several intermediate grindings. Black compound like $BaCu_3O_4$ or $Ba_2Cu_3O_5$ is formed during this process. Right amount of Tl_2O_3 was then added, pressed in to a pellet and kept in a tubular furnace already heated to about 900 °C under flowing oxygen. The pellet was kept for 2–5 min and quenched in air to room temperature and used for studies.

Still higher T_c of 125 K was reported [29] in quick succession in the same compound with stoichiometry $TlCa_2Ba_2Cu_3O_x$ (Tl-2223) quite analogous to Bi-2223 compound. The unit cell of this compound is bcc tetragonal containing three Cu perovskite like units separated by bilayers of TlO. T_c ranges between 118 and 125 K depending on the preparation parameters. Another compound with composition $Tl_2Ba_2Ca_1Cu_2O_x$ (2212) is a bulk superconductor with $T_c = 95$–108 K. This compound has two Cu perovskite units similar to Bi-2212 compound.

Figure 3.15 shows how T_c increases with the number of CuO layers from one to three. Tl compounds can be expressed with the general formula $Tl_2Ba_2Ca_{n-1}Cu_nO_{2n+4}$ and are tetragonal with two Tl-O layers and n Cu-O layers. T_c values are 80 K, 110 K and 125 K for three compounds with $n = 1$, 2 and 3, respectively. T_c is found increasing with the increase of Cu-O layers only up to $n = 3$. T_c decreases for $n > 3$. Tl being a toxic material, no attempts have been made to

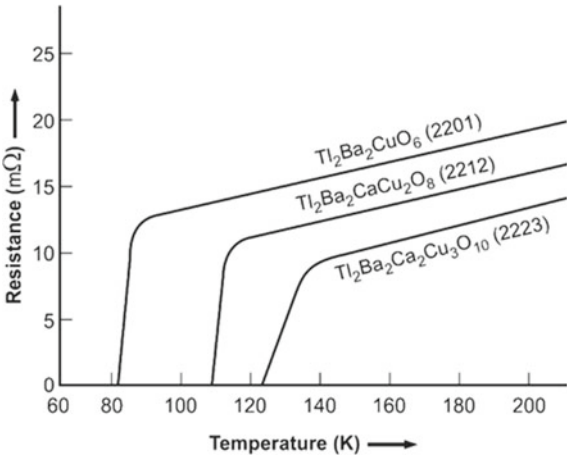

Fig. 3.15 Superconducting transition in three compositions of Tl compounds, viz.; 2201, 2212 and 2223. T_c increases with the number of Cu perovskite units 1, 2 and 3, respectively

produce wires/tapes of this material either on a laboratory scale or on a commercial scale for applications.

3.5 The Hg-Ba-Ca-Cu-O System

After a lull of about 5 years, once again a new superconductor was discovered with T_c of 94 K by Putillin et al. [30] in a compound $HgBa_2CuO_{4+y}$ or simply called Hg-1201 (as Ca is absent). This is very high T_c in contrast to the similar Tl-1201 compound which has a T_c of < 10 K. This compound has one Cu-O_2 sheet. Mercury compounds can in general be described by a formula of the type $HgBa_2Ca_{n-1}Cu_nO_{2n+2+y}$ where n can take different values starting from 1 onwards. Soon superconductivity was discovered at 130 K by Schilling et al. [31] in a multiphase Hg-compound with $n = 1$, 2 and 3. Soon the pure phase $HgBa_2Ca_2Cu_3O_{8+\delta}$ was synthesized with $n = 3$ and a $T_c = 135$ K was obtained. The unit cell structure of the three Hg-compounds with $n = 1$, 2 and 3 are shown in Fig. 3.16. Evidently, c-axis increases with the number of CuO_2 layers. Analogous to Tl-system, Hg-system too has a tetragonal structure with 'a' and 'c' parameters as given in the figure for the three phases. An enhancement in T_c with pressure in copper containing superconductors with hole conductivity is well known. Chu et al. [32] reported a T_c of 153 K for the compound $HgBa_2Ca_2Cu_3O_{8+\delta}$ (1223) at a pressure of 150 kbar. In a systematic study, Gao et al. [33] found continuous increase in T_c of all the Hg-compound (1201, 1212 and 1223) up to a pressure of 45 GPa, viz.; 164 K for 1223, 154 K for 1212 and 118 K for the compound 1201. Antipov et al. [34] report that the T_c values increase with increasing pressure for all the Hg-compounds with $n = 1, 2, 3$ and 4 as shown in Fig. 3.17. In all the compounds T_c increases with pressure and tends to saturate at high pressure. It has been conjectured that it may be possible to get T_c values as high as 164 K under

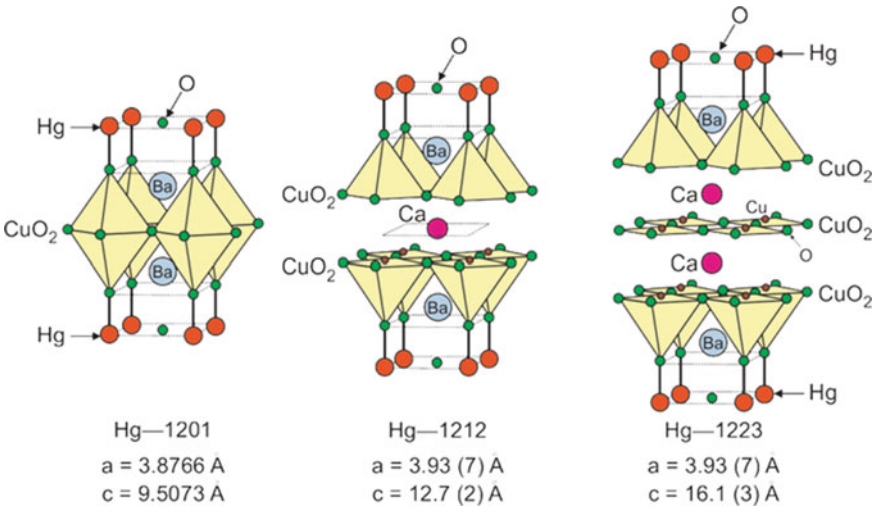

Fig. 3.16 Unit cell structure of $HgBa_2CuO_{4+\delta}$ (1201), $HgBa_2Ca_1Cu_2O_{6+\delta}$ (1212) and $HgBa_2Ca_2Cu_3O_{8+\delta}$ (1223) with one, two and three CuO_2 layers, respectively [34]. With permission from IOP

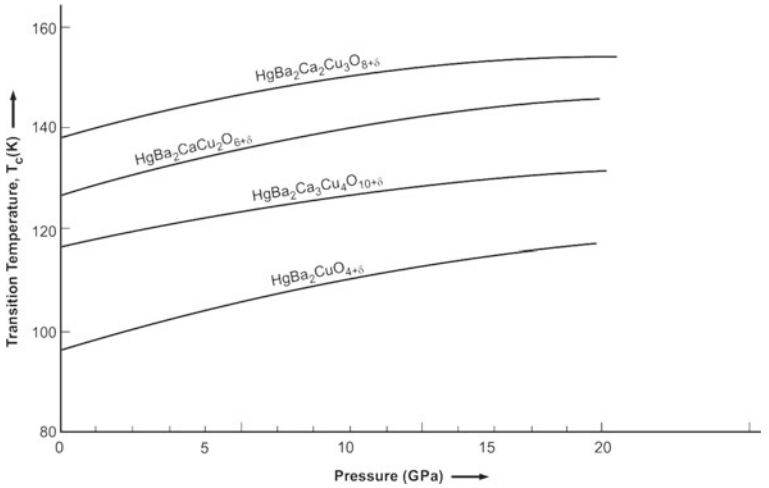

Fig. 3.17 T_c increases with pressure for Hg-compounds and with the number of CuO_2 layers up to $n = 3$. T_c decreases with pressure for compound Hg-1234 ($n = 4$). T_c is thus highest for Hg-1223 ($n = 3$) [34]. With permission from IOP

ambient pressure in optimally doped compounds through substitution if the Cu-O distances can stabilize.

Synthesis of Hg-compound is little complicated because of the toxicity of Hg and decomposition of HgO in to Hg and oxygen at comparative low temperature (430 °C). Samples are prepared in sealed quartz ampoules or in platinum or gold containers to prevent reaction. The synthesis is a two-step process. In the first step, stoichiometric mixture of barium carbonate (oxalate, nitrate or oxide), copper and calcium oxides is prepared and annealed at 600–1000 °C in air, oxygen flow or vacuum. The precursor so prepared is extremely hygroscopic and absorb CO_2 fast. All the operations are therefore carried out in a dry box. HgO is then added to the mixture and sealed in an ampoule for further annealing. T_c of these compounds has been found extremely sensitive to the presence of carbon and steps should therefore be taken to avoid carbon contents in the starting materials. An excellent topical review on the structure and synthesis of Hg-compounds has been written by Antipov et al. [34] on Hg-compounds. Hg-compound wires and tapes have not been exploited commercially for applications.

3.6 Flux Vortices, Critical Current Density and Flux Pinning in High-T_c Superconductors

The irreversible magnetic properties and critical current in type II superconductors especially in anisotropic HTS involve numerous complex mechanisms. A pure type II superconductor is well defined with T_c, B_{c1} and B_{c2} values which are the intrinsic properties of the material but same is not true for critical current density, J_c which can change widely with defects which are influenced by the fabrication process. Because of the high T_c, the J_c of HTS is also affected by thermal activation which in turn leads to flux creep and a power law I–V characteristic so that J_c is determined by an arbitrary electric field criterion. Further, J_c controls the irreversible magnetic properties of type II superconductors that are explained by the Bean critical state model [35, 36] and already discussed in Chap. 2. J_c thus is an extrinsic property of a superconductor.

Let us recall that a type II superconductor, in mixed state, ($B_{c1} < B < B_{c2}$) is threaded by flux lines each carrying a flux quantum ($\Phi = 2 \times 10^{-15}$ T m^2) or the vortices which form a triangular lattice as proposed by Abrikosov [37] and shown in Fig. 3.18. The vortices are produced by the circulating current flowing in a direction opposite to the surface screening current. The vortex is a normal cylindrical core of radius, ξ and has a region of suppressed order parameter (ψ or n_s) which is zero at the centre of the vortex. The magnetic flux at the core spreads out in the material over a distance of ~ 2λ as shown in the figure. Most interesting thing that one notices from this figure is that current in type II superconductors is carried by the entire bulk of the material unlike the type I superconductors in which the current flows only

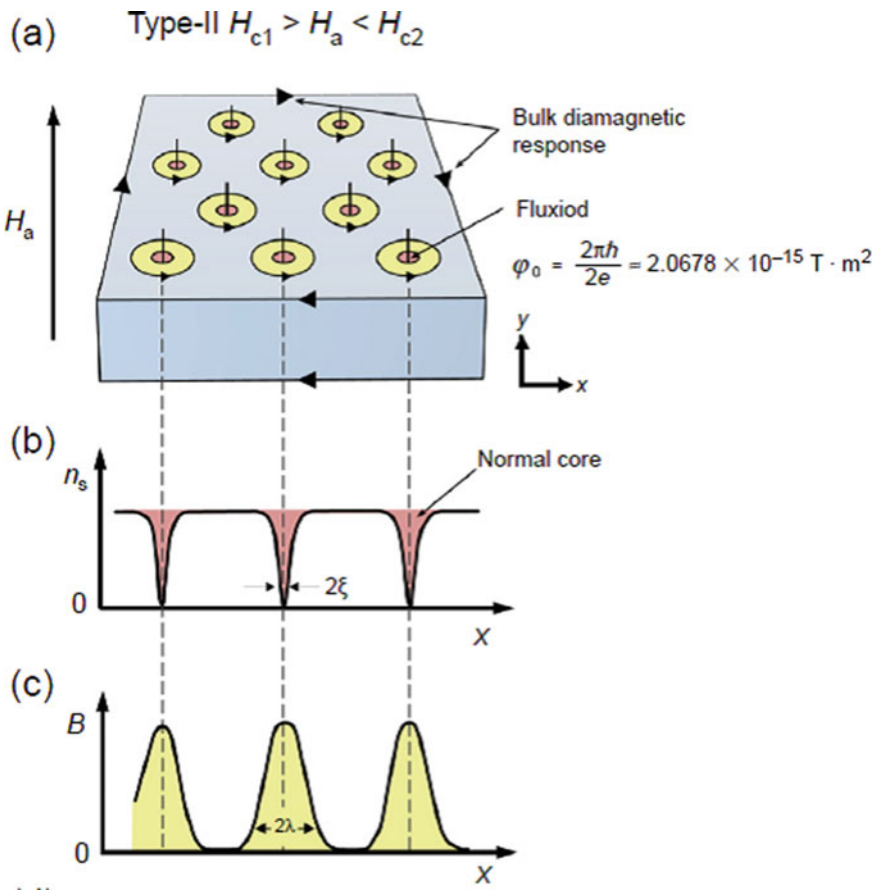

Fig. 3.18 **a** Type II superconductor in mixed state ($B_{c1} < B < B_{c2}$) is threaded by flux lines(normal cores) of dia. 2ξ, produced by current vortices flowing in a direction opposite to surface screening current along the periphery. **b** Magnetic field at the core spreads over a distance 2λ. Order parameter (ψ or n_s) drops to zero at the centre of the cores. **c** Variation of the magnetic flux density. With permission from Elsevier, 'Fundamentals of Superconductivity by C M Rey and A P Malozemoff'

through a small surface thickness (~ λ). Further, J_c in these materials is controlled by defects which may act as flux pining centres and increase J_c to high values.

Let us see how J_c in type II superconductors is controlled by defects and can be enhanced by great margin. From Ampere's law:

$$\nabla x\ B = \mu_0 J \tag{3.4}$$

Which for one dimension, reduces to:

$$\mathrm{d}B/\mathrm{d}x = \mu_0 J \tag{3.5}$$

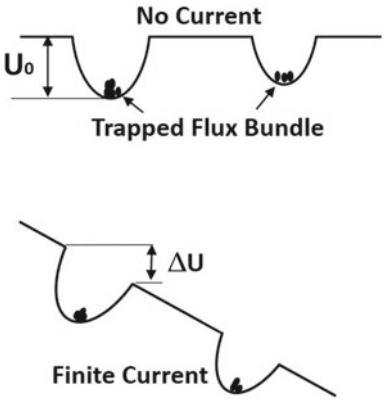

Fig. 3.19 Pinning potential without current flow (top curve) and with current flow (bottom curve). The potential wells display slope proportional to driving force when a current flows. This reduces the effective depth of the well. *Courtesy* Ajit Nandawadekar

It turns out from this expression that a supercurrent can flow in a superconductor if the field (flux line bundle) enters the bulk material and a gradient in flux line density exists. In a defect-free superconductor, however, Abrikosov lattice is in an equilibrium state. A gradient can only be created by introducing defects that will pin the flux lines. The pinning centres are represented by potential wells (Fig. 3.19) of average depth U_0 and width a. Bundle of flux quanta with an average flux $n\Phi_0$ are captured by the potential well. When no current flows, the probability of flux leaving the potential well is proportional to Boltzmann factor:

$$P_0 \propto \exp(-U_0/k_B T) \tag{3.6}$$

When a current of density J flows through the superconductor the potential acquires a slope (Fig. 3.19) proportional to the driving Lorentz force $F \propto n\Phi_0 J$. The slope is equivalent to a reduction in the effective potential well depth to $U = U_0 - \Delta U$

$$\text{Here } \Delta U \approx n\ \Phi_0 J a\ \ell \tag{3.7}$$

where ℓ is the length of the flux bundle. The increased probability of the escape of the flux P is now given by:

$$P = P_0 \exp(+\Delta U/k_B T) \tag{3.8}$$

The flux line gradient grows steeper, following Ampere's law, if the current density is increased in the type II superconductor. This generates increasing Lorentz force which at a certain maximum value overcomes the pinning force and starts pushing the flux lines out of their defect potential wells. As already discussed in Chap. 2, this current density is the critical current density J_c at which the pinning force, F_P becomes equal to the Lorentz force, F_L ($= B \times J_c$). Thus, the pinning force

in a defect superconductor can be determined from the measurement of J_c at a given field and at a given temperature. This flux pinning force, however, can be increased by introducing pinning centres such as dislocations, voids, secondary phase precipitations or elemental additions to the material. For illustration, we present some flux pinning data from Selvamanickam's group [38] on YBCO films as shown in Fig. 3.20. The figure shows field dependence of flux pinning force, F_P ($B//c$) at 4.2 K for 7.5 and 15 mol.% Zr-doped YBCO films. The flux pining force increases to an ultra-high value = 1.7 TN/M^3 for film doped with 15% Zr which is twice the value obtained for the film doped with 7.5% Zr. Surprisingly, the pinning force (F_P) does not show a drop with increasing field between 8 and 31 T ensuring high-current density in doped films right up to 31 T.

High pinning performance in these doped films has been attributed to spontaneous formation of the $BaZrO_3$ (BZO) defect columns during film growth.

When current through a type II superconductor exceeds J_c the flux lines or the vortices start moving and there is a sharp jump in the voltage in the I–V plots. This sharp jump in the voltage gets smeared if J_c distribution within the superconductor is not homogeneous. The right kind of J_c distribution can however cause a power law dependence $V \sim I^n$ [39], where the power index n is a function of inhomogeneity distribution in the material. Such a power law curve can also arise from flux creep, which is particularly relevant to HTS materials. Very high J_c values have been achieved in all the practical superconductors including HTS like the 2G YBCO-coated conductors [40] following innovative fabrication techniques and introducing efficient pinning centres. Naturally occurring pinning centres, like dislocations, voids, stacking faults, crystal twin boundaries, chemical precipitates, and such

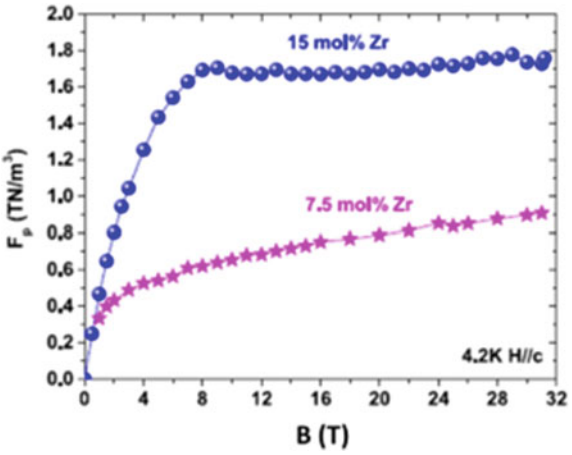

Fig. 3.20 Flux pinning force, F_P ($B//c$) at 4.2 K plotted against magnetic field for 7.5 and 15 mol.% Zr-doped YBCO films. Note ultra-high F_P = 1.7 TN/M^3 for film doped with 15% Zr. There is hardly a drop of F_P between 8 and 31 T field ensuring high-current density in field up to 31 T. With permission from V. Selvamanickam; Open access under CCA, A. Xu et al. App. Phys. Lett., MATERIALS **2**, 046111 (2014), http://dx.doi.org/10.1063/1.4872060

other defects, provide much of the pinning force. Pinning centres are also introduced by creating particular type of defects in to the substrate which get replicated in to the epitaxially grown films. Radiation-induced defects too can increase the number of pinning centres and increase the magnitude of the pinning force, F_P as reported by Weber [41].

3.7 Critical Surface of High-T_c Superconductors

The mixed state of HTS reveals the existence of a well-defined irreversibility temperature (T_{irr}) up to which magnetic irreversibility persists. This temperature is a characteristic feature of a superconductor and depends on the applied field. T_{irr} can be determined [42] from zero-field cooled (ZFC) and field cooled (FC) magnetization as a function of temperature plots as shown in Fig. 3.21. Magnetic irreversibility in these materials originates from the movement of vortices overcoming the pinning force. Below T_{irr}, the vortices are trapped by the pinning centres.

Above T_{irr} the system is magnetically reversible due to high thermal energy. When temperature is lowered below T_{irr}, many of the grains become coupled and strong irreversibility effects are observed in the magnetization curve. An irreversible line can be plotted from the reversibility data obtained on a superconductor sample as a function of field (B) and temperature (T). The critical surface of a HTS thus looks like [43], the one shown in Fig. 3.22. The irreversible line separates high-temperature magnetically reversible region from low temperature magnetically irreversible region. In conventional metal superconductors with low T_c, the critical surface is very close to the upper critical field B_{c2} and the critical current density J_{co} which is unaffected by flux creep. In HTS, the critical surface is diminished and shifts downwards as indicated by the arrows. The critical surface is now bound by the irreversibility line $B_{irr}(T)$ and

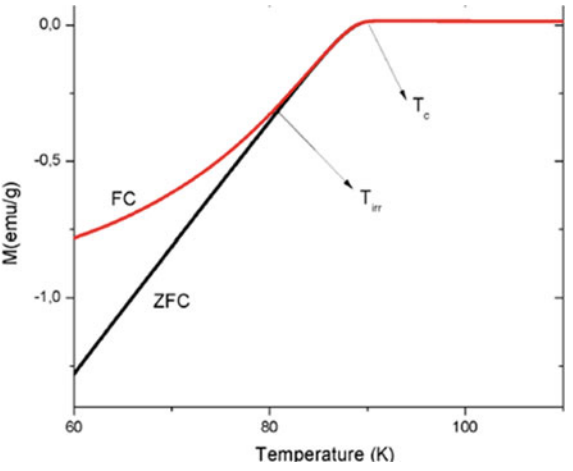

Fig. 3.21 Typical zero-field cooled (ZFC) and field cooled (FC) magnetization of a $Y_{0.6}Lu_{0.4}Ba_2Cu_3O_{7-\delta}$ sample as a function of temperature [42]. With permission from Armando Sarmiento Santos, Escuela de Física—UPTC; Open Access under CCA, Journal of Physics: Conference Series **480**, 012036 (2014), http://dx.doi.org/10.1088/1742-6596/480/1/012036

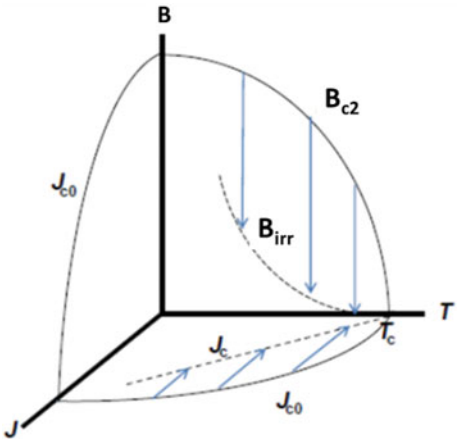

Fig. 3.22 Typical critical surface bound by of field B, temperature T and current density J in a HTS within which, a supercurrent can persist. The superconducting parameters, however, shrink because of thermal activation and flux creep as shown by arrows. The critical surface now is bound by B_{irr} line and the flux-creep-reduced critical current density, $J_c(T)$ [43]. With permission from Elsevier

the critical current density $J_c(T)$ which is now reduced by flux creep. Nevertheless, the energy gap and the vortex current around the vortices persist within the bulk of superconductor until B_{c2} is reached. Between B_{c2} and B_{irr} the vortices are in a liquid-like state called a 'vortex liquid'. Below B_{irr}, the vortices are in a disordered state if the pinning centres are disordered and the state is called a 'vortex glass state'.

3.8 The Depairing Current

The critical current density of a superconductor as a function of temperature and magnetic field is the most important parameter for building a superconducting device. Large efforts have continuously been made to enhance the critical current in practical superconductors largely through new fabrication techniques and by adding effective pinning centres. There is however a theoretical thermodynamic limit beyond which critical current density cannot be raised. We have learnt in Chap. 2 that a normal to superconducting phase transition is of the second order (no latent heat involved) and the free energy is reduced. Now consider the transport current in a superconductor. Contrary to this decrease in energy during the normal to superconducting transition, the kinetic energy of the electron pairs (Cooper pairs) increases as the transport current increases. At a certain high enough current value, this increase in energy may exceed the decrease in energy while entering the superconducting state. It would then be favourable for a superconductor to get back to normal state. This current is called the depairing current, J_d. This is the upper theoretical limit of the maximum current density that can be achieved in a superconductor no matter how strong is the flux pinning. We can thus define depairing current density as the current density at which the kinetic energy of the electron pair is equal to the binding energy of the pair. Beyond this current, the energy gap vanishes and superconductivity is completely destroyed. The depairing current J_d thus becomes an intrinsic critical parameter

together with T_c, J_c and B_{c2} characterizing a superconductor. A rough estimation of J_d can be made [44] from the London equations by equating the kinetic energy of the pair with the free energy density;

$$\frac{1}{2} n_s m^* v_s^2 = \frac{B_c^2}{2\mu_0} \tag{3.9}$$

Substituting $v_s = \frac{J_s}{2en_s}$ and $n_s = \frac{m^*}{4\mu_0 e^2 \lambda^2}$

$$J_d = \frac{B_c}{\mu_0 \lambda} \tag{3.10}$$

The above equation is only an approximation because n_s has been assumed here to remain unaffected by the current approaching J_d which is not realistic. The equation however establishes the fact that J_d is strongly dependent on critical magnetic field and the penetration depth. Similar expression has been derived for type II superconductors following the Ginzberg–Landau theory yielding:

$$J_d(0) = 5.56 \times 10^{-3} \times \frac{\sqrt{B_{c2}(0)}}{\lambda^2(0)} \tag{3.11}$$

where J_d is in A/m^2, B_{c2} is in Tesla and λ is in metres. The theoretical limit of J_d can only be reached in samples with very high pinning force with J_d approaching 10^{12}–10^{13} A/m^2.

For almost all applications, only three critical parameters, T_c, J_c and B_{c2} of a superconductor are considered routinely and not the J_d. In fact, J_d is hardly measured partly because of the technical difficulties related to excessive heating and burnt out of samples at high currents. Also, at very high current, the critical temperature, T_c too shifts to lower temperature. Most measurements are therefore carried out using short-pulse currents with short duration of about 50 ns to prevent burnt out of the samples. For example, the depairing current density in $YBa_2Cu_3O_{7-x}$ is of the order of 10^8 A/cm^2 (4.2 K), and therefore, ultra-thin films of $YBa_2Cu_3O_{7-x}$ patterned to microbridges have been used to allow for an effective heat transfer into the MgO substrate. Arpaia et al. [45] measured J_d in YBCO nanowire with a protecting gold capping layer. They measured multiple YBCO bridges with cross sections as small as 50×50 nm^2 and reported $J_d = 1 \times 10^8$ A/cm^2 in bridges covered with Au capping. The measured J_d is found to be close to values predicted by Ginzburg–Landau theory.

3.9 Grain Boundary Problem in High-T_c Superconductors

High-T_c superconductors are not only characterized by high T_c and high B_{c2} but also by poor grain connectivity and strong anisotropy of superconducting properties along

the *a*–*b* (CuO_2) planes and along the *c*-axis. Lack of perfect stoichiometry especially the oxygen content is another problem. Critical current density, J_c depends strongly on the method of preparation as well. For example, J_c in bulk YBCO, prepared by solid-state diffusion method, and remains confined to 10^3 A/cm^2 at 77 K. In melt textured samples, where number of grain boundaries (GB) decrease, J_c increases and can reach a value of 10^5 A/cm^2 (77 K). It increases further to 10^6 to 10^7 A/cm^2 in epitaxial films with preferred grain orientation. Chaudhuri et al. [16] did report high J_c in epitaxially grown YBCO films and Dinger et al. [17] reported similar high J_c values in YBCO single crystals. Inter-grain J_c, however, was found to be very small which turned out to be a stumbling block in realizing high transport J_c in bulk material and in wires and tapes prepared by powder-in-tube (PIT) method.

Large anisotropy in these ceramic superconductors is another difficulty which needs resolution. Widely different coherence lengths in YBCO along the *a*–*b* plane, $\xi_{ab} = 1$–2 nm and along the *c*-axis, $\xi_c = 0.3$ nm lead to anisotropy in various superconducting properties including J_c which now depends on the crystallographic orientation of the grains. Misorientation of grain reduces inter-grain $J_{c(GB)}$ and larger the misorientation angle greater is the reduction in $J_{c(GB)}$. In fact, several factors are responsible for poor quality of grain boundaries (GB) which are dependent upon the process followed for the synthesis of this ceramic superconductor. Two HTSs which have been pursued for application are the BSCCO and YBCO superconductors. The third one, Bi-2212 is also close to commercial production. For operation at 77 K in magnetic field, BSCCO (2223) tapes are preferred because of its higher $T_c = 110$ K and better flux pining properties. The popular approach to make YBCO tape wires is the so-called coated conductor technique in which the superconductor is deposited on a textured tape substrate with *c*-axis normal to the direction of current flow. These 2G REBCO-coated conductors now have very high J_c. The polycrystalline films, however, have severe problem of the inter-grain interfaces (GB). Misalignment of the *a* and *b* axes of more than a few degrees causes week links similar to Josephson junctions with critical current significantly lower than inside the bulk grain. The grain boundary problem has been solved at least partially through a variety of techniques to be described in Chap. 6.

3.10 Discovery of Superconductivity in Magnesium Diboride (MgB_2)

Over a thousand condensed matter physicists presented their work on the newly discovered superconductor, Magnesium Diboride (MgB_2) [46] on 12 March 2001 at the American Physical Society meeting held in the Grand Ballroom of the Westin Hotel in Seattle. The session lasted for more than 5 h. Most surprising part of the discovery has been that MgB_2 was a known material since 1953 and yet it had to wait for nearly 50 years to be known as a superconductor, with a $T_c = 39$ K. Studies on this material proceeded at great speed and within a few years physics of this material was

well understood. Soon, the material positioned itself as a practical superconductor [47, 48] to be used at 20 K with superconducting parameters superior to Nb_3Sn. Long lengths of multifilamentary MgB_2 wires and tapes with increased J_c and B_{c2} are being manufactured now and used for magnets and other applications. MgB_2 has several advantages over HTSs. It is inexpensive and wire fabrication does not need costly silver. Its T_c is 39 K and thus has an operational window of 20–30 K. Magnets and other devices can thus be conduction cooled and operated using closed-cycle refrigerators (CCR). Some other advantages can be summarized as below:

- A number of diborides are known [49] to be superconducting but with only within a T_c range of 0.62 K (NbB_2) and 9.5 K (TaB_2). Only MgB_2 has the highest T_c of 39 K.
- There are no grain boundaries weak links in MgB_2 restricting the critical current to low values like in HTSs. Standard powder-in-tube (PIT) technique is employed to manufacture long lengths of wires/tapes. This is in contrast to 2G-coated conductors which need very sophisticated thin film deposition techniques which makes it very expensive.
- It has much smaller anisotropy of upper critical field compared to HTS. $\frac{B_{c2}^{ab}}{B_{c2}^{c}}$ in MgB_2 is just 1.1–1.7.
- Enhancement of transport critical current continues to be made. MRI scanners using MgB_2 magnets (0.5 T) are already in the market. 3 T MRI scanner might hit the market sooner than expected.
- MgB_2 has low density, 2.57 g/cc and is thus a potential candidate for space-oriented superconducting applications.

3.10.1 Peculiar Properties of MgB_2

Magnesium diboride, MgB_2, a low cost material, known since 1953, was found superconducting when cooled to 39 K by Nagamatsu [46] in 2001. The original plots of magnetic susceptibility versus temperature under zero-field cooled (ZFC) and field cooled (FC) conditions and the electrical resistivity versus temperature are shown in Fig. 3.23a and b, respectively. Both the measurements confirm a sharp superconducting transition at 39 K. MgB_2 though is considered to be a superconductor of conventional type, nevertheless, has peculiar properties. The material is characterized by two widely differing energy gaps. The presence of two energy gaps has been theoretically understood by assuming two species of electrons at the Fermi surface in its electronic structure, namely the 'sigma-bonding' and the pi-bonding electrons. Using the measured values of the two energy gaps 6.8 and 1.8 meV for sigma and pi bands, respectively and employing BCS theory the sigma and pi bands of electrons are found to have two coherence lengths, 13 and 51 nm, respectively. The corresponding penetration depths are 47.8 and 33.6 nm. The Ginzberg–Landau (G-L) parameter κ turns out to be =3.68 for sigma-bonding and 0.66 for pi-bonding. The first term is more than $1/\sqrt{2}$ and the second term less than $1/\sqrt{2}$. Thus, the

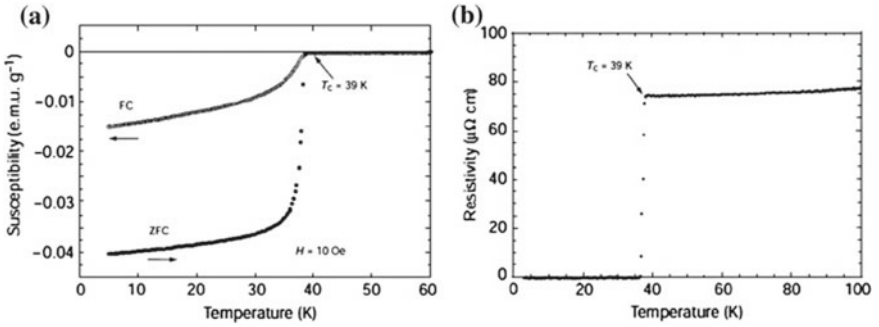

Fig. 3.23 **a** Magnetic susceptibility versus temperature plots of MgB_2 under zero-field (ZFC) and field cooled (FC) conditions. **b** The electrical resistivity versus temperature plot for MgB_2. Both the measurements show a sharp superconducting transition at 39 K [46]. With permission from Nature Publishing Group

sigma-bonding superconductivity is of type II and the pi-bonding superconductivity of the type I. MgB_2 has been termed by some as a superconductor of 'one and a half' (1.5) type [50].

3.10.2 Crystal and Electronic Structure and Energy Gaps in MgB_2

MgB_2 is a metal with a layered hexagonal structure where the B atoms form a graphite-like honeycombed layers and the magnesium atoms sit at the centre of the hexagons in between the boron planes as shown in Fig. 3.24. The electronic states at the Fermi level are mainly either σ or π-bonding boron orbitals. The σ-bonding states

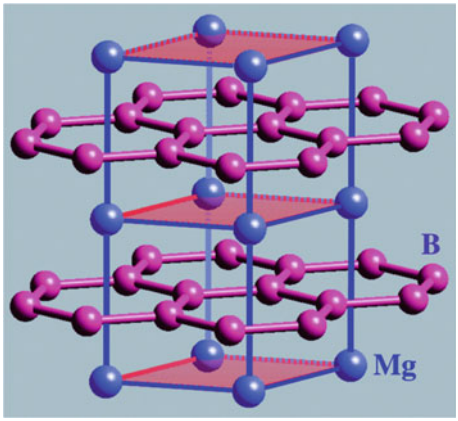

Fig. 3.24 B atoms form a graphite-like honeycombed layers and the magnesium atoms occupy the centre of the hexagons in between the boron planes (Taner Yildirin, Materials Today, **5**, 40 (2002) ISSN:1369 7021 © Elsevier Science Ltd 2002Open access under CBY-NC-ND license)

are confined in the boron planes and couple very strongly to the in-plane vibration of boron atoms. Based upon the strong-coupling formalism of superconductivity by Eliashberg, Choi et al. [51] showed from the first principle that this strong-coupling results in strong electron-pair formation of the σ-bonding states with an energy gap of 6.8 meV. This pairing is strong and confined to the boron planes and Fermi surface partially. This strong pairing, in fact, is the principal contribution responsible for the occurrence of superconductivity in MgB_2. The π-bonding states, on the remaining parts of the Fermi surface form much weaker pairs with an energy gap of 1.8 meV. This pairing is enhanced by the coupling with σ-bonding states. MgB_2 though has high T_c nevertheless is similar to conventional metal superconductors. It remains metallic all through unlike the cuprates which are insulators without doping. The major difference with metal superconductors is that MgB_2 is characterized by two energy gaps corresponding to two types of pairing.

Choi et al. [51] carried out calculations and obtained numerical values of the two energy gaps and their effects on the measurable parameters. They were successful in accounting for the high T_c, the anomalous specific heat versus temperature behaviour and for the isotopic behaviour. The calculated energy gaps versus temperature plots are shown in Fig. 3.25. As seen in the figure the energy gap corresponding to σ-bonding states is large, 6.8 MeV which drops with increasing temperature and faster close to T_c than the smaller energy gap (1.8 MeV) corresponding to the π-bonding states. Both the energy gaps, however, merge and disappear at T_c. The experimental energy gap parameters fit well with the calculated values. The temperature variation of the energy gaps can be expressed by the following equation:

$$\Delta(T) = \Delta(0)\left[1 - \left(\frac{T}{T_c}\right)^p\right]^{1/2} \tag{3.12}$$

here $p = 2.9$ for the larger energy gap corresponding to the σ-bonding states and $p = 1.8$ for the smaller energy gap corresponding to the π-bonding states. This

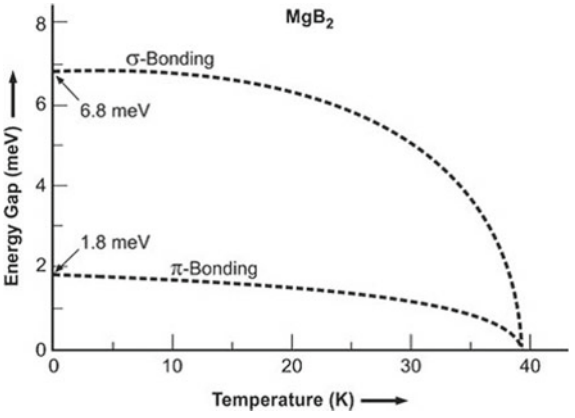

Fig. 3.25 Two superconducting energy gap parameters plotted against temperature. Both the gaps merge and become zero at T_c [51]. With permission from Nature Publishing Group

temperature variation of the energy gaps has been verified experimentally through tunnelling, optical and specific heat measurements. Parameter $2\Delta(0)/k_B T_c$ for the σ-bonding comes out to be =4.0 and for the π-bonding 1.06, k_B being the Boltzmann constant. Two-gap superconductivity was also inferred from measurements using Raman spectroscopy, photoemission, penetration depth and tunnelling. That MgB_2 is a BCS type conventional superconductor, with an intermediate to strong s-wave coupling, has been borne out by a plethora of experimental data. The existence of Cooper pairs with charge 2e has been confirmed through AC and DC Josephson effect [52] studied on break junctions of MgB_2. Observation of isotope effect in this material, to be discussed in the next section, further confirmed the role of phonons in the formation of the Cooper pairs and the occurrence of superconductivity. Because of comparative ease, studies on MgB_2 have been fast and very passionate. Studies were carried out on almost all aspects of this material and a very large number of papers published. Two widely different energy gaps arise from a weak electron–phonon coupling in the 3D π-bands (smaller gap) and a strong coupling in 2D σ-band (larger gap). In MgB_2, the two sets of electrons do interact, though weakly, through Coulomb repulsion and scattering from states in one band to states in the other band. That, such a weak interaction can cause both the bands go superconducting at the same temperature with two widely different energy gaps, is the striking property of this superconductor.

3.10.3 The Boron Isotope Effect

One single most credible evidence of BCS type superconductivity is the observation of isotope effect which confirms the phonon mediated Cooper pair formation mechanism. As per the classical form of the BCS theory [53], the isotope coefficient α in the formula $T_c \propto M^{-\alpha}$ is 0.5. Here M is the atomic mass of the element. The Boron isotope effect was reported by Budko et al. [54] as early as 2001. Careful resistivity and magnetization experiments were performed on two types of bulk samples, viz.: $Mg^{10}B_2$ and $Mg^{11}B_2$ by exposing isotopic pure ^{10}B and ^{11}B to magnesium vapours. Figure 3.26 is the plot of resistivity of MgB_2 against temperature [55]. It shows a resistive superconducting transition close to 40 K. The upper insert shows the effect of replacing ^{10}B by ^{11}B in MgB_2 on the resistive T_c and the lower inset on magnetization T_c. In both the experiments, T_c is found to reduce by 1 K, that is, from 40.2 K for $Mg^{10}B_2$ to 39.2 K for $Mg^{11}B_2$. The value of exponent α for boron isotope in MgB_2, comes out to be $=0.26 \pm 0.03$. This value is quite close to the values found in YNi_2B_2C and $LuNi_2B_2C$ borocarbides. No isotope effect was observed when ^{24}Mg was substituted for ^{25}Mg. It thus appears that only boron phonons take part in pair formation. There are indications that high-frequency boron A1g optical modes are responsible for the onset of superconductivity in MgB_2.

For a BCS superconductor, a $T_c = 39$ K is considered high. Looking at the BCS expression for T_c one finds that T_c depends upon the phonon energy, $\hbar\omega$, the electron density of states $N(0)$ and the electron–phonon interaction parameter V. The phonon

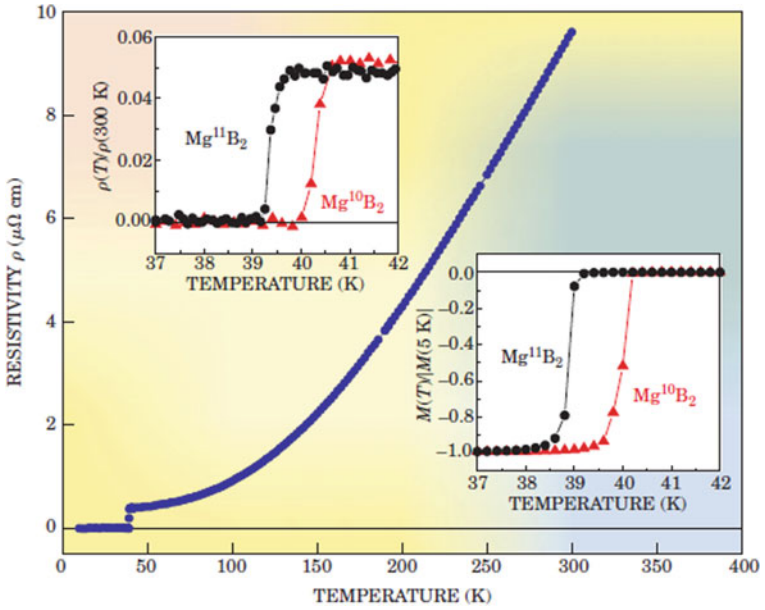

Fig. 3.26 Resistive superconducting transition in MgB_2 at 40.2 K. Upper inset: Effect of replacing $^{10}B_2$ by $^{11}B_2$ on the resistive T_c in MgB_2. The resistivity has been normalized to 300 K Lower inset: Effect of replacing $^{10}B_2$ by $^{11}B_2$ in MgB_2 on T_c through magnetization experiments. The data have been normalized to -1 at 5K. The transition temperature, T_c of MgB_2 is reduced by 1 K when $^{10}B_2$ is replaced by $^{11}B_2$ as confirmed by both the types of experiments [55]. Reproduced from 'Physics Today, 56, 34 (2003), with the permission of the American Institute of Physics'

energies of MgB_2 are indeed high

$$kT_c = 1.14\hbar\omega \exp\left[-\frac{1}{N(0)V}\right] \tag{3.13}$$

but so are the energies of other borides and light element binary alloys but all have low T_c. The density of states is low because MgB_2 does not have d-electrons. The only other parameter left, which may lead to high T_c, is the strong electron–phonon interaction represented by 'v'. Perhaps, the selective coupling between the specified electron states and specified phonons is responsible for high-T_c (~ 40 K) superconductivity.

3.10.4 Some Physical Properties of MgB_2

We briefly describe some physical properties and interesting studies that have been carried out on this material. The Hall effect measurements by Elstev et al. [56] on MgB_2 single crystal reveal that it has two types of charge carriers, holes in the plane

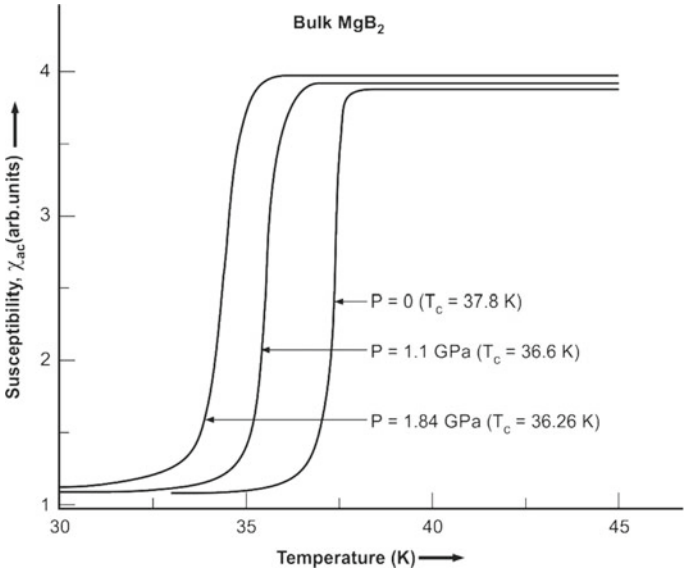

Fig. 3.27 Plots of AC susceptibility of bulk MgB_2 against temperature at different pressure up to 1.84 GPa. T_c shifts to lower temperature with increasing pressure [57]. With permission from the American Physical Society. http://journals.aps.org/prb/abstract/10.1103/PhysRevB.64.012507

and electrons along the *c*-axis. There is anisotropy in electrical resistivity along the plane and in the perpendicular direction such that $\rho_c/\rho_{ab} = 3.5$. Normal state Hall coefficient is positive in plane (*B*//*c*, *I*//*ab*) and negative in the out-of-plane (*B*//*ab*, *I*//*c*) confirming that the electronic structure of MgB_2 is multiband.

Pressure is another important parameter which has been exploited to study this material. Lorenz et al. [57] have made detailed studies on ac susceptibility and Seebeck coefficient with increasing pressure up to 1.84 GPa. T_c always decreases with increasing pressure and is linear with pressure. As shown in Fig. 3.27, T_c drops down with the increase of pressure till the highest pressure of 1.84 GPa. This drop in T_c is rather fast at a rate of $-$ 1.6 K/GPa and is close to the theoretically calculated value of $-$ 1.4 K/GPa.

The Seebeck coefficient has been found to be positive and relatively small. It decreases with the decrease of temperature similar to in a metal with hole-type carriers. Substitution at Mg as well as B sites with a host of elements always resulted in the decrease of T_c. Some of the materials tried are C, Al, Li, Si, Be, Cu, Mn, Nb, Ti, Fe, Co, Ni and Zn. Decrease in T_c is severe in case of substitution with Mn, Co and C and slow with Si and Li. Least decrease in T_c occurs with Zn substitution. The coherence length values, as calculated from B_{c2}, range between 6.1 and 6.5 nm in ab plane and between 2.5 and 3.7 nm along the *c*-axis. The most accurate data for a single crystal gives $\xi_{ab}(0) = 6.1$–6.5 nm and $\xi_c(0) = 2.5$–3.7 nm. The penetration depth as evaluated from B_{c1} values range between 85 and 203 nm. The lower critical magnetic field (B_{c1}) as reported by several investigators range from 25 to 48 mT.

Upper critical magnetic field B_{c2} has been reported for material in different forms like bulk, single crystal and thin films and in different orientations over a wide range of values ranging from 2.5 to 32 T. The highest value of B_{c2}, 32 T has been reported for films with $T_c = 39$ K. Higher $B_{c2} = 40$ T has been reported by Patnaik et al. [58] for films with lower T_c. B_{c2} drops almost linearly with increasing temperature saturating at low temperature. The B_{c2} anisotropy ratio $= B_{c2}^{ab}/B_{c2}^{c} = 1.1-1.7$ is reported for textured bulk and partially oriented crystallites. Higher ratio = 1.8–2.0 has been reported [58] for c-axis oriented MgB_2 film. The irreversible field extrapolated to 0 K, range from 6 to 12 T for MgB_2 in bulk, thin film, powder, tape and wire. B_{irr} thus is $=0.5\ B_{c2}$ in MgB_2 instead of $=0.8\ B_{c2}$ for conventional low temperature superconductors. Impurity additions are known to increase B_{c2} in type II superconductors as the mean free path is reduced and so does the coherence length $\xi(0)$. Braccini et al. [59] do report significant enhancement of B_{c2} in C-alloyed MgB_2 films irradiated with He-ions. The disorder thus introduced, raises in-plane B_{c2} to 51 T (4.2 K) and along the c-axis to 35 T (4.2 K). These are very promising values and show the potentiality of use of this material with high J_c in high magnetic field. Extrapolation of data to $T = 0$ K shows that B_{c2}^{ab} might lead to paramagnetic limit of 70 T. Various properties of MgB_2 that we have discussed in the preceding sections are summarized below and also tabulated in Table 3.4.

Table 3.4 Important superconducting parameters of MgB_2

Parameter	Unit	Value
Crystal structure		Hexagonal AlB2-type
Unit cell parameter	Å	$a = 3.14326 \pm 0.0315$ $c = 3.51936 \pm 0.0323$
Isotope coefficient for Boron, α_B in $\left(T_c \propto M^{-\alpha}\right)$		$\alpha = 0.266 \pm 0.03$
Transition temperature, T_c	K	39
Penetration depth, λ	nm	85–203
Coherence length, ξ_{ab}	nm	6.1–6.5
Coherence length, ξ_c	nm	2.5–3.7
Coherence length, ξ_{ab} single crystal	nm	6.1–6.5
Coherence length, $\xi_c(0)$ single crystal	nm	2.5–3.7
Lower critical field, H_{c1}	mT	25–48
Highest upper critical field (film)	T	32–40
$\frac{H_{c2}^{ab}}{H_{c2}^{c}}$ anisotropy (textured bulk/partially oriented crystallites)		1.1–1.7
Irreversible field, H_{irr} (0 K)	T	6–12
Energy gap (σ band)	meV	6.8
Energy gap (π-band)	meV	1.8
Room temperature resistivity	$\mu\Omega$ cm	10
Resistivity close to T_c	$\mu\Omega$ cm	0.5
Estimated paramagnetic limited field, B_{c2}^{ab}	T	70

3.10.5 Summery of the Various Properties of MgB_2

- Transition temperature T_c always decreases with elemental substitution at Mg and B sites and is more severe in case of substitution with Mn, Co and C but moderate with Si and Li. Least decrease in T_c occurs with Zn substitution.
- Most reliable coherence length values in a single crystal come out to be $\xi_{ab}(0) =$ 6.1–6.5 nm and $\xi_c(0) = 2.5$–3.7 nm.
- The penetration depth as evaluated from B_{c1} values range between 85 and 203 nm.
- The lower critical magnetic field B_{c1}, as reported by different groups range from 25 to 48 mT.
- Upper critical magnetic field B_{c2} has been reported for MgB_2 in its different forms like bulk, single crystal and thin films and in different crystal orientations in the range of 2.5–40 T. The highest value of $B_{c2} = 40$ T has been reported by Patnaik et al. [58] for films with lower T_c.
- B_{c2} drops almost linearly with increasing temperature and saturating at low temperature.
- The B_{c2} anisotropy ratio, $\frac{B_{c2}^{ab}}{B_{c2}^{c}} = 1.1-1.7$ is for textured bulk and partially oriented crystallites.
- Higher ratio, $\frac{B_{c2}^{ab}}{B_{c2}^{c}} = 1.8-2.0$ has been reported [58] for c-axis-oriented MgB_2 film.
- B_{irr}, the irreversible magnetic field extrapolated to 0 K, range from 6 to 12 T for MgB_2 in bulk, thin film, powder, tape and wire. B_{irr} thus is $=0.5\ B_{c2}$ in MgB_2 instead of $=0.8\ B_{c2}$ for conventional low T_c superconductors.
- B_{c2} of type II superconductors is known to increase with the increase of normal state resistivity as the mean free path is reduced and so does the coherence length $\xi(0)$.
- Braccini et al. [59] report significant enhancement of B_{c2} in C-alloyed MgB_2 films irradiated with He-ions. The disorder thus introduced, raises in-plane B_{c2} to 51 T (4.2 K) and B_{c2} along the c-axis to 35 T (4.2 K).

The critical parameters of MgB_2 are very impressive and have already been exploited commercially and are being used for a variety of conduction-cooled magnets. Conduction-cooled MgB_2 magnet-based MRI scanners are expected to flood the market in very near future. We will devote a full chapter (no. 7) on the fabrication techniques of MgB_2 wires and cables planned to be used in superconducting magnet projects. Table 3.4 summarizes the important superconducting parameters of MgB_2.

3.11 The Discovery of Iron-Based Superconductors—LaFeAsO 1111 Compounds

One more surprise came from the Japanese group, Kamihara et al. [60] headed by Hideo Hosano when they reported a high T_c of 26 K in iron-based oxypnictides, of the type $La(O_{1-x}F_x)FeAs$ layered superconductor containing magnetic materials like Fe, Co and Ni. Iron was earlier believed to be an enemy to superconductivity. Here, the contradiction was between the static spin ordering in iron and the dynamic formation of Cooper pairs (electrons with opposite spins) in a superconductor. In $La(O_{1-x}F_x)FeAs$, x varies from 5 to 12%. The crystal structure of this superconductor [61] is shown in Fig. 3.28. The conduction layers Fe_2As_2 are sandwiched between the insulating La_2O_2 layers. It has a tetragonal structure of the type (ZrCuSiAs) with p4/nmm space group. The room temperature lattice parameters of the undoped samples are $a = 0.403552(8)$ nm and c = 0.87263(3) nm. The lattice constants decrease with F-doping. Thus, for example, the lattice parameters for 5% F-doping are: $a = 0.40320(1)$ nm and $c = 0.87263(3)$ nm. The electrical resistivity of $La(O_{1-x}F_x)FeAs$ is plotted against temperature up to 40 K as shown in Fig. 3.29. The undoped sample does not show superconductivity down to the lowest temperature. Highest value of T_c (= 26 K) is obtained for 11 at% F-doped sample. Higher doping leads to a drop in T_c. Superconductivity was not observed when doping was done with Ca^{2+} instead of with F. This gives a strong signal that superconductivity is induced by electron (F^-)-doping and not by hole (Ca^{2+})-doping. The material LaOFeAs was prepared following the solid-state method. Powders of dehydrated La_2O_3, lanthanum arsenide and iron arsenide were thoroughly mixed and sealed in a silica tube filled with Ar-gas. The tube was heated to 1250 °C for 40 h. Right quantities of CaO and

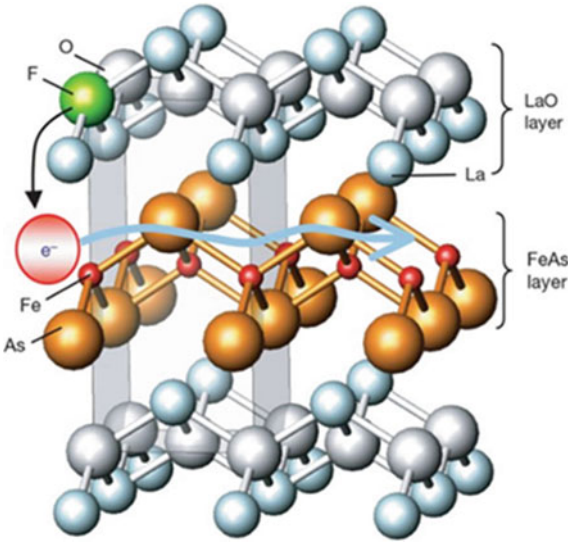

Fig. 3.28 Crystal structure of LaFeAsO, 1111 compound. The Fe_2As_2 conduction layers are sandwiched between the insulating La_2O_2 layers. The structure is of the type (ZrCuSiAs) electron carriers generated by F^- doping at the oxygen site are transferred to FeAs conduction layer [61]. Reproduced with the permission from Springer Nature

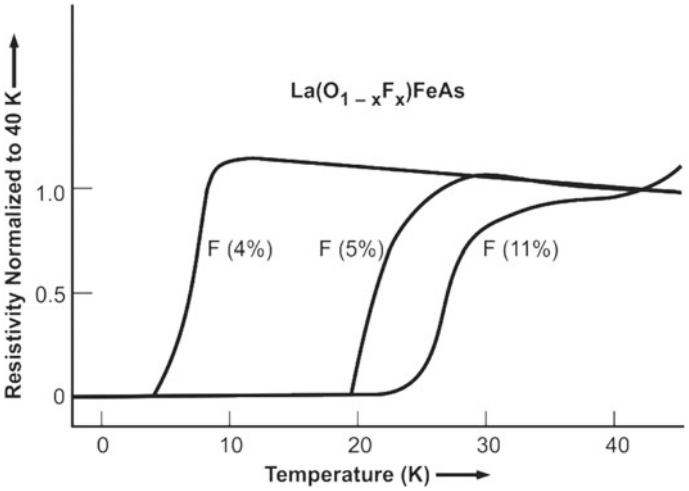

Fig. 3.29 Electrical resistivity plotted against temperature for $La(O_{1-x}F_x)FeAs$ for 0, 4, 5 and 11%) of F-doping [60]. With permission from American Chemical Society

1:1 mixture of LaF_3 and La were added to the starting material for doping with Ca^{2+} and F^-, respectively. This was followed again by the same heating schedule.

3.11.1 High T_c (> 50 K) in Sm and Nd-Based Oxypnictides

Significantly, high values of T_c have been reported for these oxypnictides by replacing La by different rare earths. For Ce-compound the T_c rises to above 40 K and above 50 K for Nd, Pr, Sm and Gd. Jaroszynski et al. [62] reported T_c higher than 50 K for their Sm and Nd-based materials. They carried out high-field studies on three REFeAsO 1111 materials with RE as La, Sm and Nd. Superconductivity was induced either by doping F at O-sites or creating O-vacancies by synthesizing O-deficient materials. Three compounds studied, viz.; $LaFeAsO_{0.89}F_{0.11}$, $SmFeAsO_{0.85}F_{0.15}$ and $NdFeAsO_{0.94}F_{0.06}$ yield $T_c = 28$ K, 53.5 K and 50.5 K, respectively. These values have been tabulated in Table 3.5. It is to be mentioned that these materials were synthesized at high pressure and high temperature following the solid-state reaction route. Pre-sintered powders of LaAs. SmAs and NdAs were mixed together with powders of Fe, Fe_2O_3 and FeF_2 in right stoichiometric proportions ground and pressed in to pellet form. The pellets were sealed in boron nitride (BN) tubes and heated at 1250 °C under 6 GPa pressure for 2 h. Interestingly, the highest values of T_c obtained for optimal doping show that the optimal level is different for different doping materials, viz.; 11%, 15% and 6% for La, Sm and Nd, respectively. A detailed review article by Aswathi et al. on oxypnictides had appeared in the literature [63].

Table 3.5 Superconducting parameters of REFeAsO 1111 oxypnictides with RE as La, Sm and Nd [62]

Parameter	Unit	$LaFeAsO_{0.89}F_{0.11}$	$SmFeAsO_{0.85}F_{0.15}$	$NdFeAsO_{0.94}F_{0.06}$
Transition temperature, T_c	K	28	53.5	50.5
Optimum doping of F	%	11	15	6
Upper critical field, B_{c2}	T	36	150	204

The upper critical field B_{c2} of La $FeAsO_{1-x}F_x$ 1111 compounds turns out to be high. The B_{c2} values as evaluated from resistive (ρ–B plots) using Werthamer–Helfend–Hohenberg (WHH) formula,

$$B_{c2} = -0.693\ T_c\ [dB_{c2}/T]_{T_c} \tag{3.14}$$

and extrapolated to 0 K for La, Sm, Nd, Pr and Ce 1111 compounds are [62] 36 T, 150 T, 204 T, 72 T and 43 T, respectively (Table 3.6). B_{c2} has been found to decrease with increasing F^- doping even though T_c shows an opposite trend. For $CeFeAsO_{0.8}F_{0.2}$, the B_{c2} is 43 T and T_c is 42.5 K and for $CeFeAsO_{0.9}F_{0.1}$ the B_{c2} value is 94 T and T_c is 38.4 K. Similar variation of B_{c2} is reported for $LaFeAsO_{1-x}F_x$. For $LaFeAsO_{0.95}F_{0.05}$, the B_{c2} is 63-65 T, and for $LaFeAsO_{0.89}F_{0.11}$, it is 36 T. Sm 1111 compound also show similar behaviour. Like the T_c of this compound, B_{c2} of the 1111 compounds also increases if the compound is prepared by high-pressure route. B_{c2} up to 230 T and T_c of 51 K have been reported [63] in $NdFeAsO_{0.82}F_{0.18}$. The field anisotropy B_{c2ab}/B_{c2c} is about five, much smaller than in YBCO compound. The values of irreversible field, B_{irr} are also correspondingly high as compared to MgB_2. Tables 3.5 and 3.6 indicate beyond doubt that these materials can have high T_c and B_{c2} once the process parameters are optimized.

In spite of high B_{c2} and high T_c, these compounds suffer from the problem of granularity similar to cuprates. Thus, the inter-grain critical current J_{cgp} is far smaller

Table 3.6 Superconducting parameters of REFeAsO 1111 oxypnictides with RE as La, Sm, Nd, Pr and Ce [66]

Oxypnictide	T_c (K)	B_{c2} (0 K)
$LaFeAsO_{0.89}F_{0.11}$	28	36
$SmFeAsO_{0.85}F_{0.15}$	53.5	150
$NdFeAsO_{0.94}F_{0.06}$	50.5	204
$PrFeAsO_{0.94}F_{0.06}$		72
$CeFeAsO_{0.8}F_{0.2}$	42.5	43
$CeFeAsO_{0.9}F_{0.1}$	38.4	94
$NdFeAsO_{0.82}F_{0.18}$ [63]	51	230

than the intragrain critical current J_{cg}. Through magneto-optical measurements (low temperature laser scanning electron microscopy) on Sm 1111 compounds, Kametani et al. [64] have shown that the transport current though is high within the grains but is low at the grain boundaries in very low field. Great advancements have been made in recent times to develop IBSC conductors and in good lengths and with high J_c. This is a significant step towards the exploitation of these materials on a commercial scale. These developments will be discussed in Chap. 8 on 'Iron-Based Practical Superconductors'.

3.11.2 Superconductivity in K-Doped $BaFe_2As_2$ 122 Compounds

A new member of the Fe-As superconductor family was discovered in 2008 raising the T_c to all time high 55 K in $SmFeAsO_{1-x}$ system. This was achieved by F^- doping or creating oxygen deficiency (electron-doping) in the Fe_2As_2 conducting layer which suppresses the structure phase transition (at 135–140 K) and induces superconductivity. Hole doping too has been reported to induce superconductivity in the $(La_{1-x}Sr_x)FeAsO$ system but the T_c was limited to 25 K.

Rotter et al. [65] discovered superconductivity first time in an oxygen-free pnictide.

A T_c of 38 K has been reported in a compound, $(Ba_{0.6}K_{0.4})Fe_2As_2$ prepared by partially replacing Ba with K. The parent compound $BaFe_2As_2$ has a tetragonal $ThCr_2Si_2$ type crystal structure with I4/mmm space group and consisting of $(FeAs)^-$ layers separated by Ba^{2+} ions as shown in Fig. 3.30. $BaFe_2As_2$ is a poor metal with Pauli paramagnetism. It shows a spin density wave (SDW) anomaly at 140 K similar to the anomaly in LaFeAsO compound at 150 K. The anomaly is accompanied with a structural and magnetic phase transition and anomalous specific heat, resistivity and susceptibility. Hole doping in $(FeAs)^-$ layers by partial substitution of K^+ on the Ba^{2+} sites suppresses this SDW anomaly and induces superconductivity. This SDW anomaly seems to be a pre-requisite for superconductivity. The structural phase transition can be suppressed by electron-doping or hole-doping in the Fe-As layer which leads to the appearance of superconductivity. Through this substitution, Rotter et al. [65] have found superconductivity in $(Ba_{0.6}K_{0.4})Fe_2As_2$ at 38 K. The resistive superconducting transition is shown in Fig. 3.31. Thus, a new category of oxygen-free Fe-As compounds was added to the list of Fe-As-based superconductors.

3.11.3 Superconductivity in Iron-Chalcogenides

After the discovery of superconductivity in Fe-oxypnictides of the type LaFeAsO, these compounds became the most studied materials with an object of getting higher T_c. Report of T_c as high as 55 K in oxygen deficient $SmFeAsO_{0.85}$ [62] inspired

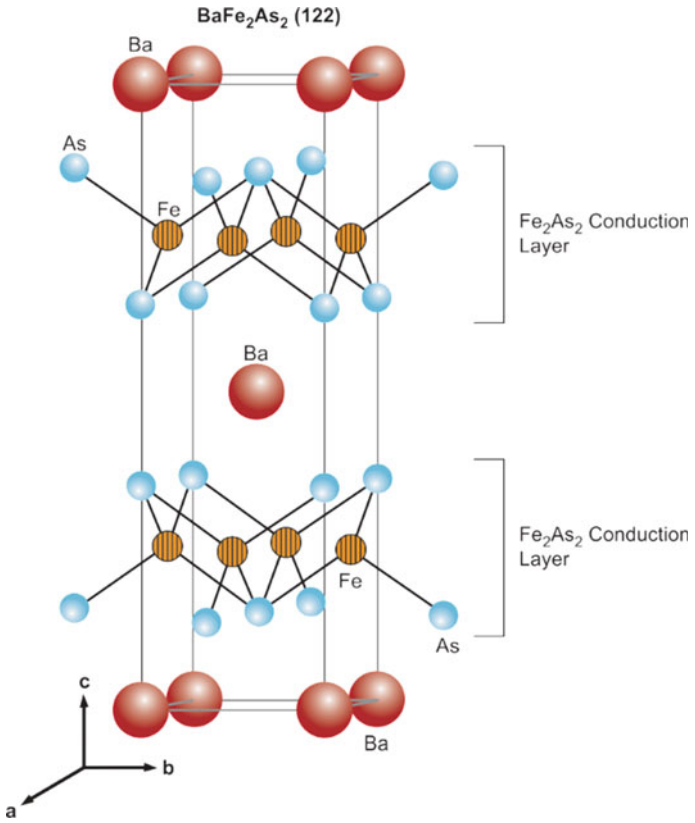

Fig. 3.30 Crystal structure of $BaFe_2As_2$ 122 compound (of the type $ThCr_2Si_2$) with space group I4/mmm [65]. With permission from APS. http://journals.aps.org/prb/abstract/10.1103/PhysRevB.82.180520

researchers to continue to look for Fe-based superconductors with still higher T_c. Superconductivity was indeed reported in a new material, Fe-Se or referred to as (11) iron-chalcogenide at 8 K by Hsu et al. [66]. This compound has a simple structure of Fe-Se layers without intercalating cations, something quite different from the oxypnictides. Static magnetic ordering too does not occur up to a pressure of 38 GPa. Tellurium doping ($FeSe_{0.42}Te_{0.58}$) raises the T_c to 15 and 37 K at high pressure. Guo et al. [67] reported superconductivity in a compound of the composition $K_{0.8}Fe_2Se_2$ at 30 K at ambient pressure. The compound was synthesized through intercalation of Fe-Se by K. Figure 3.32 shows the crystal structure of this compound. Single crystal grown by flux method shows a tetragonal structure with $a = 3.9136(1)$ Å and $c = 14.0367(7)$ Å and space group I4/mmm. Obviously, the intercalation increases the c-axis parameter significantly. The carrier density as evaluated from Hall effect measurement turns out to be $1.76 \times 10^{21}/cm^3$. The Hall coefficient R_H is negative and constant above 105 K. The electrical conduction is thus electron dominated.

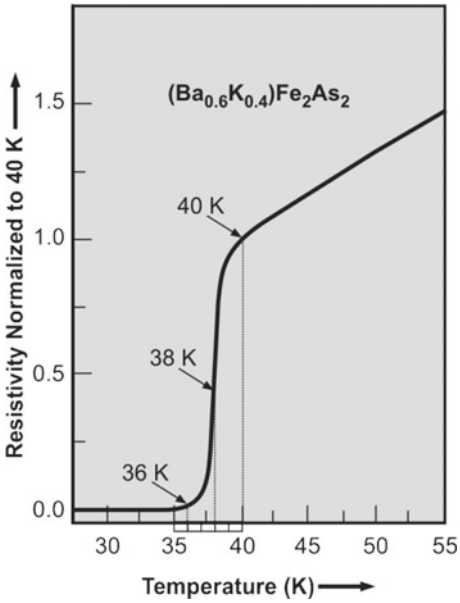

Fig. 3.31 Resistive superconducting transition in $(Ba_{0.6}K_{0.4})Fe_2As_2$ [65]. With permission from APS. http://journals.aps.org/prb/abstract/10.1103/PhysRevB.82.180520

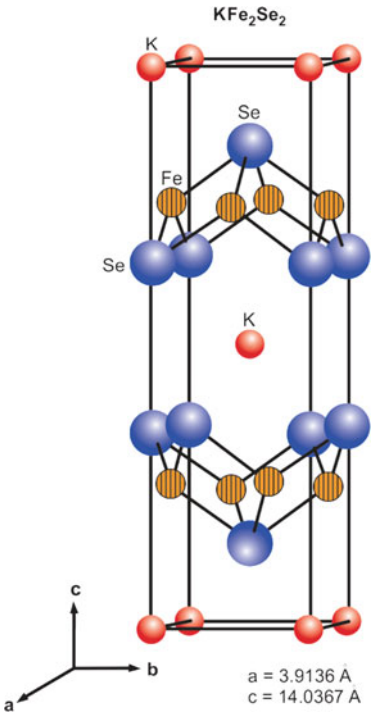

Fig. 3.32 Crystal structure of KFe_2Se_2 of the type $(ThCr_2Si_2)$ $a = 3.9136(1)$ Å and $c = 14.0367$ Å [67]. With permission from APS. http://journals.aps.org/prb/abstract/10.1103/PhysRevB.82.180520

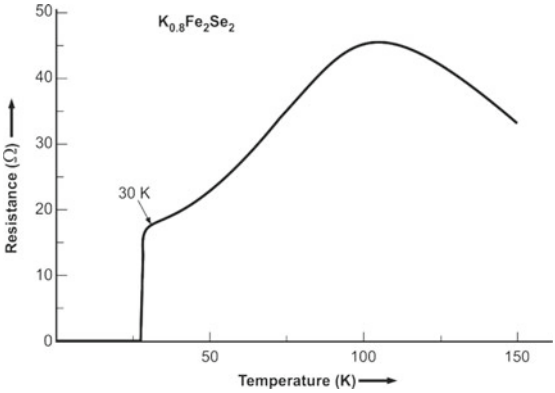

Fig. 3.33 Resistance–temperature behaviour of $K_{0.8}Fe_2Se_2$, below 150 K. Superconducting transition occurs at 30 K [67]. With permission from APS. http://journals.aps.org/prb/abstract/10.1103/PhysRevB.82.180520

The compound has a semiconductor behaviour in electrical resistivity between room temperature and 105 K below which it turns metallic and finally superconducting (at 30 K). The resistive transition of the $K_{0.8}Fe_2Se_2$ compound is shown in Fig. 3.33. The lower critical magnetic field B_{c1} and upper critical magnetic field B_{c2} have been calculated to be 0.2 T and 9 T, respectively.

The superiority of IBSCs over HT cuprates in many respects made them very attractive materials for research as well as for exploiting them for practical applications especially the high-field magnets. The deluge of papers that appeared within the first year of the discovery by Hosono is the testimony to the potential of these superconductors. The structural phase transition in these IBSC is very interesting. The interplay between the superconductivity and antiferromagnetic ordering (SDW) is quite fascinating. At the same time, the $J_c = 10^5$ A/cm^2 (4.2 K, 10 T) in these materials has already crossed the threshold of practical conductors. We will therefore discuss these IBSCs again in a separate Chap. 8 in greater detail.

3.12 Superconductivity at 203 K in Sulphur Hydride (H_3S)

After attaining a T_c well above 100 K in cuprates the next target for discovery became the room temperature superconductor. Luckily, the Eliashberg formulation of the BCS theory does not envisage an upper limit to T_c in a superconductor. A high-T_c BCS superconductor needs (i) high phonon frequency, (ii) very strong electron–phonon interaction and (iii) high density of states per spin per atom. Ashcroft [68] focused on hydrogen the lightest atom which has very high vibrational frequency and provides strong electron–phonon interaction. Mcmahon et al. [69] made calculations and predicted that metallic hydrogen should show superconductivity at 100–140 K in molecular phase and 300–350 K in atomic phase at a pressure of 500 GPa. Even though no superconductivity has been detected in hydrogen yet, several hydrogen-rich covalent hydrides like SiH_4, SnH_4 and H_2S were chosen for

studies. Hydrogen has high Debye temperature and thus high Debye frequency ($\theta_D = \hbar\omega_D/k_B$). Combining hydrogen with the heavier elements may also help to induce superconductivity as they contribute to low frequency known to enhance electron–phonon interaction. Besides, very high pressures needed to metallize pure hydrogen are no longer needed. Drozdov et al. [70] investigated H_2S which showed metallicity at ~ 96 GPa which improves further with increasing pressure. At 200 GPa, it has a resistivity of 3×10^{-7} Ω. They also observed that H_2S gets dissociated in to H_3S and elemental S, a favourable situation indeed. Superconductivity was confirmed with the observation of Meissner effect. Magnetic susceptibility measurements show a sharp transition from the diamagnetic to paramagnetic state for zero-field-cooled (ZFC) sample at T_c. Drozdov et al. [71] reported a record onset T_c of 203 K. Magnetization measurements reveal a pronounced hysteresis which indicated that it is a type II superconductor. The lower critical field B_{c1} is found to be < 30 mT. The T_c of sulphur hydride rises sharply as the pressure exceeds 150 GPa as shown in Fig. 3.34a. The T_c of the sulphur deutride stays lower than the T_c of the hydride at all pressures as expected in a BCS superconductor. Figure 3.34b shows the resistive superconducting transition at 185 K and 90 K, respectively, for the sulphur hydride and sulphur deutride. Highest T_c reported by Drozdov et al. for the sulphur hydride is 203 K [71]. Figure 3.34c shows the temperature dependence of the magnetization of sulphur hydride at 155 GPa in zero-field cooled (ZFC) and 20 Oe field cooled (FC) modes. The magnetization measurements clearly show an onset of superconductivity at 203 K. Optical micrograph of the sulphur hydride at 155 GPa is shown in the inset.

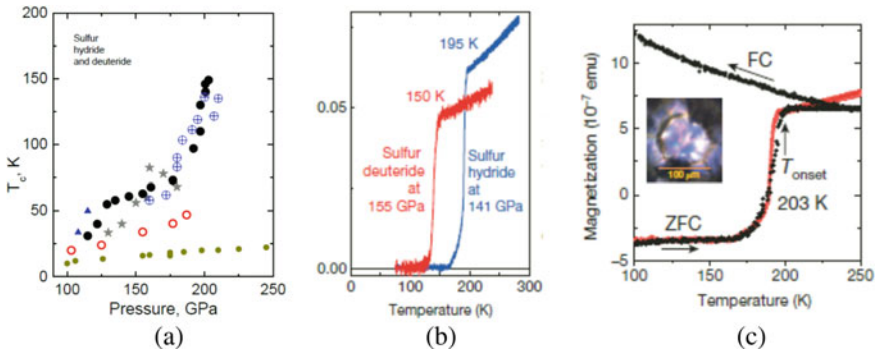

Fig. 3.34 **a** Dependence of T_c of sulphur hydride (different runs) and sulphur deutride (open circles) with pressure. Note the sharp rise of T_c at $p > 150$ GPa. T_c of sulphur deutride in the entire pressure range is lower than the T_c of sulphur hydride. The bottom plot (small circles) is for pure sulphur. **b** Superconducting transition at 150 K (@ 155 GPa) in sulphur deutride and at 195 K (@ 141 GPa) in sulphur hydride. **c** The temperature dependence of the magnetization of sulphur hydride at 155 GPa in zero-field cooled (ZFC) and 20 Oe field cooled (FC) modes. The $T_{c\ onset}$ is 203 K. Optical micrograph of the sulphur hydride at 155 GPa is also shown in the inset under cooled conditions [71]. With permission from Springer Nature

The synchrotron X-ray diffraction measurements by Einaga et al. [72] confirmed the presence of hydrogen-rich hydride, H_3S phase which is responsible for the emergence of superconductivity. It turned out that H_2S (D_2S) dissociates in to H_3S (D_3S) and elemental sulphur under high pressure $3H_2S \rightarrow 2H_3S + S$. The authors report that the compound in normal state as well as in superconducting state has the same structure as revealed from the XRD data obtained at room temperature and at low temperatures. Two superconducting phases with bcc structures have been identified. One with a crystal structure which correspond to R3m symmetry as shown [73] in Fig. 3.35a and b. This phase has a T_c of 120 K and is called the low T_c phase. Second phase appears when pressure increases to 150 GPa. This phase, called the high-T_c phase, has a structure with Im-3M symmetry (Fig. 3.35c) and is responsible for the

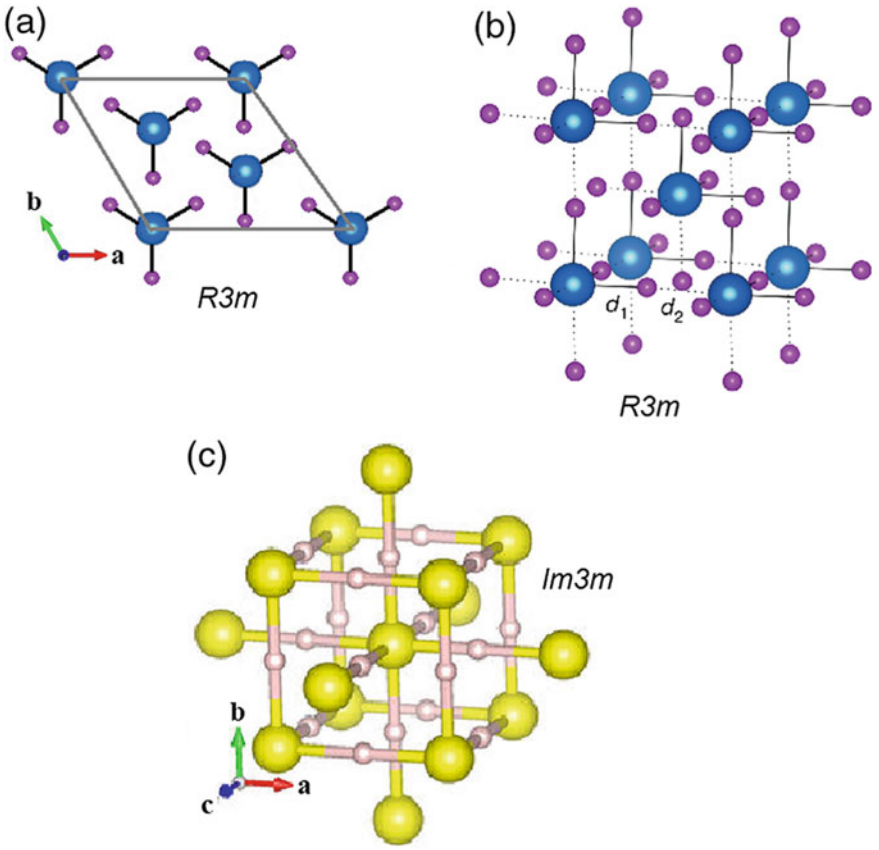

Fig. 3.35 Structures of the low T_c phase with R3m symmetry and $T_c = 120$ K (**a**) top view—large spheres are sulphur atoms and small spheres hydrogen (**b**) side view; one can see that d1 $\neq d_2$, d_i ($i = 1.2$) are the distances between the H ion and neighbouring S ions. **c** Structure of the Im-3m high-T_c (200 K) phases [73]. With permission from Am. Phys. Soc.

record $T_c \approx 203$ K. Even though the transition temperature increases with pressure, yet the structure does not change within a pressure range of 92–173 GPa. This appears contradictory to the sharp jump observed at 150 GPa in H_3S and 160 GPa in D_3S (Fig. 3.34 c). It is seen from this figure that the pressure dependence of T_c is different in the R3m phase at lower pressures and in the Im-3m phase at higher pressures. X-ray diffraction data are however found to be the same in the two phases and differ only in ordering of hydrogen atoms in the two pressure domains. It has been conclusively proven that the highest critical temperature of 203 K corresponds to the Im-3m phase of H_3S. The pressure dependence of T_c, however, reverses after the $T_{c\,max}$ has been reached. The T_c decreases upon further increase in pressure. This decline is however slow indicating that the pressure dependence of T_c is strongly asymmetric with respect to $T_{c\,max}$, which is somewhat unusual.

It will be of interest to look for other hydrides which may turn superconducting at still high temperature and possibly at room temperature. Indeed, many groups have carried out theoretical calculation and have predicted superconductivity with high T_c in several hydrides. Peng et al. [74] and Wang et al. [75] made many interesting predictions based on their theoretical calculations. Thus, for example, Wang et al. predicted superconductivity in calcium hydride, CaH_6 at 240 K, Li et al. [76] in YH_6 at 264 K. Feng et al. [77] also predicted superconductivity in MgH_6 at 264 K at a pressure of > 300 GPa. There are others who have predicted room temperature superconductivity but the moot question is that can we realize superconductivity which would be stable at ambient pressures which is a requirement of a practical superconductor.

3.13 Superconductivity at Room Temperature ($T_c = 288$ K @ 267 GPa)

The group led by Mikhail Eremets at the MPI for Chemistry, Mainz, Germany reported [78] still higher T_c of 250 K in LaH_{10} within the Fm3m structure at a pressure of 170 GPa. Superconductivity was confirmed through the observation of zero-resistance, isotope effect, and the dependence of T_c on external magnetic field. These magnetic field measurements yielded a value of the upper critical magnetic field B_{c2} (0 K) as ~ 120 T. This 50 K jump in T_c in hydrides gave strong indications that room temperature superconductivity is achievable using high pressure technique.

The record of $T_c = 250$ K in LaH_{10} too was broken in the following year (2020) by a team led by Ranga Dias of university of Rochester, USA [79] when the team reported an all-time high T_c of ~ 288 K in a compound containing C, H and S at a pressure of 267 GPa. Dias technique had merit in so far as the LaH_{10} was formed at high temperature by Drozdov et al. [78] but Dias used a milliwatt green laser into the diamond anvil cell (DAC) containing C-H-S mixture for several hours at 4GPa pressures before raising the pressure further. Their DAC also contained probes that recorded electrical resistance dropping to zero and confirmed superconductivity

through magnetic measurements. The Dias's team added a third component C to the sulphur hydride system in the hope to observe more structures and more chances to find higher T_c.They succeeded and discovered superconductivity almost at room temperature (RT), that is, 288 K (15 °C). The composition of the compound could not be ascertained but is believed to be in the range of CSH_6 to CSH_8.

A resistive sharp superconducting transition is observed in the C-H-S compound as shown in Fig. 3.36a. The T_c increases with increasing pressure and the highest T_c = 288 K is obtained at a pressure of ~ 267 GPa. Fig.3.36b shows the microphotographs of the sample during the photochemical process. The electrical leads in a four-probe configuration for resistance measurements can also be seen in the microphotograph. As seen from Fig. 3.36c T_c rises gradually with increasing pressure from 140 GPa up to a pressure of 220 GPa when a T_c = 194 K is reached. As the pressures is increased further T_c rises rather sharply until a highest value of 288 K is attained at a pressure of 267 GPa. The T_c of the samples was determined from the electrical resistance (R) and a.c. susceptibility (χ) measurements. A discontinuity appears at around 225 GPa between the two pressure regimes at which the rise of T_c with pressure becomes sharper. This method of pressure induced metallization followed by superconductivity thus appears to be a promising route to room temperature superconductivity. The next challenge will be to find an alternate route perhaps a chemical route to mimic such high pressure during the synthesis of material and yet realize room temperature superconductivity at ambient pressure.

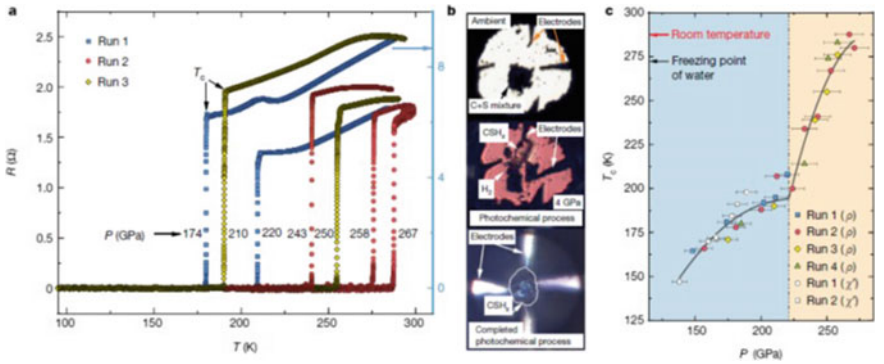

Fig. 3.36 **a** Resistive superconducting transition in C-H-S compound at different pressures. Highest T_c is obtained at ~ 288 K at a pressure of ~ 267 GPa. The vertical (R) axis on right is for two samples measured in a separate experimental run (shown by arrow). **b** Microphotographs of the samples during photochemical process in the C–S–H compound. Electrical leads in a four-probe configuration for resistance measurements are also shown. **c** Pressure dependence of T_c, as determined from the electrical resistance (R) and a.c. susceptibility (χ) measurements. Highest T_c = 288 K is observed for a pressure of 267 GPa (With permission from Springer Nature)

References

1. J.R. Gavaler, Appl. Phys. Lett. **23**, 480 (1974)
2. L.R. Tastardi, J.H. Wernick, W.A. Royer, Solid State Commun. **15**, 1 (1974)
3. J.G. Bednorz, K.A. Muller, Z. Phys. B: Condens. Matter **64**, 189 (1986)
4. D.C. Johnston, H. Prakash, W.H. Zachariasen, R. Viswanathan, Mater. Res. Bull. **8**, 777 (1973)
5. A.W. Sleight, J.L. Gillson, F.E. Bierstedt, Solid State Commun. **17**, 27 (1975)
6. C.W. Chu, P.H. Hor, R.L. Meng et al., Phys. Rev. Lett. **58**, 405 (1987)
7. R.J. Cava, R.B. van Dover, B. Batlogg, E.A. Rietman, Phys. Rev. Lett. **58**, 408 (1987)
8. R.P.Aloysius, Ph.D. Thesis, 2002, Cochin University of Science & Technology, Cochin
9. M.K. Wu, J.R. Ashburn, C.J. Torng et al., Phys. Rev. Lett. **58**, 908 (1987)
10. R.G. Sharma, Y.S. Reddy, S.R. Jha, S.S. Dubey, Pramana—J. Phys. **30**, L-81 (1988)
11. S.R. Jha, Y.S. Reddy, D.K. Suri, K.D. Kundra, R.G. Sharma, Deepak Kumar, Pramana—J. Phys. **32**, 277 (1989)
12. A. Pandey, R. Rajput, B. Sarkar, Y.S. Reddy, R.G. Sharma, Physica C **256**, 335 (1996)
13. A. Pandey, Y.S. Reddy, R.G. Sharma, J. Mater. Sc. **32**, 3701 (1997)
14. R.G. Sharma, S. Lahiry, A. Pandey, D. Bhattacharya, Bull. Mater. Sci. **22**, 265 (1999)
15. R.G. Sharma, Y.S. Reddy, S.R. Jha, Rev. Solid State Sci. **2**, 409 (1988)
16. P. Chaudhuri, R.H. Koch, R.B. Laibowitz et al., Phys. Rev. Lett. **58**, 2684 (1987)
17. T.R. Dinger, T.K. Worthington, W.J. Gallagher, R.L. Sandstorm, Phys. Rev. Lett. **58**, 2687 (1987)
18. H. Maeda, Y. Tanaka, M. Fukutomi, T. Asano, Jpn. J. Appl. Phys. **27**, L665 (1987)
19. M. Takano, J. Takada, K. Oda et al., Jpn. J. Appl. Phys. **27**, L1652 (1988)
20. B. Sarkar, Y.S. Reddy, R.G. Sharma, Mater. Res. Bull. **28**, 629 (1993)
21. S.R. Shukla, D.K. Pandya, N. Kumar, S.K. Sharma, R.G. Sharma, Physica C **219**, 483 (1994)
22. S.R. Shukla, Y.S. Reddy, N. Kumar, S.K. Sharma, R.G. Sharma, Pramana—J. Phys. **41**, 285 (1993)
23. H. Maeda, K. Innoue, T. Kiyoshi, T. Asano et al., Physica B **216**, 141 (1996)
24. M. Tachiki, S. Takahashi, Solid State Commun. **70**, 291 (1989)
25. K. Kadowaki, *Electronic Properties and Mechanism of High T_c Superconductors*, ed. by T. Oguchi, K.Kadowaki, T. Sasaki (North-Holland, Amsterdam, 1992), p. 209
26. M. Kikuchi, N. Ayai, T. Ishida et al., SEI Tech. Rev. No. **66**, 73 (2008)
27. Z.Z. Sheng, A.M. Hermann, Nature **332**, 55 (1988)
28. Z.Z. Sheng, A.M. Hermann, Nature **332**, 138 (1988)
29. S.S.P. Parkin, V.Y.Lee, E.M. Engler et al., Phys. Rev. Lett. **60**, 2539 (1988)
30. S.N. Putillin, E.V. Antipov, O. Chmaissem, M. Marezio, Nature **362**, 226 (1993)
31. A. Schilling, M. Cantoni, J.D. Guo, H.R. Ott, **363**, 56 (1993)
32. C.W. Chu, L. Gao, F. Chen et al., Nature **365**, 323 (1993)
33. L. Gao, Y.Y. Xue, F. Chen et al., Phys. Rev. **B50**, 4260 (1994)
34. E.V. Antipov, A.M. Abakumav, S.N. Putillin, Supercond. Sci. Technol. **15**, R-31 (2002)
35. C.P. Bean, Phys. Rev. Lett. **8**, 250 (1962)
36. C.P. Bean, Rev. Mod. Phys. **36**, 31 (1964)
37. A. A. Abrikosov, Zh. Eksperim. i. Fiz. **32**, 1442 (1957); Sov. Phys.—JETP **5**, 1174 (1957)
38. A. Xu, L. Delgado, N. Khatri, Y. Liu, V. Selvamanickam et al., Appl. Phys. Lett. Mater. **2**, 046111 (2014)
39. W.H. Warnes, D.C. Larbalestier, Cryogenics **26**, 643 (1986)
40. A.P. Malozemoff, Y. Yamada, in *100 years of Superconductivity*, ed. by H. Rogalla, P. Kes (CRC Press, Taylor & Francis Group, Boca Raton, FL, 2012), p. 689e702
41. H.W. Weber, Int. J. Mod. Phys. E **20**, 1325e1378 (2011)
42. J.F. Cepeda Grimaldos, M.V. Chiquillo, G.I. Supelano, D. Martínez et al., J. Phys.: Conf. Ser. **480**, 012036 (2014)
43. C.M. Ray, A.P. Malozemoff, Chapter 2, *Superconductors in Power Grid—Materials and Applications* (Woodhead Publishing Series in Energy, 2015), pp. 29–73

44. M. Liang, Depairing Current Density of Cuprate Superconductors. Ph.D. Thesis, University of South Carolina, USA (2013)
45. R. Arpaia, S. Nawaz, F. Lombardi, T. Bauch, IEEE Trans. Appl. Supercond. **23**, 1101505 (2013)
46. J. Nagamatsu, N. Nakagawa, T. Muranaka et al., Nature **410**, 63 (2001)
47. P.C. Canfield, S.L. Budko, Sci. Am. **292**, 80 (2005)
48. S.L. Budko, P.C. Canfield, Physica C **514**, 142 (2015)
49. N. Varghese, Ph.D. Thesis, Cochin University of Science & Technology, Cochin, India
50. V.V. Moshchalkov, M. Menghini, T. Nishio, Q. Chen, A. Silhanek et al., Phys. Rev. Lett. **102**, 117001 (2009)
51. H.J. Choi, D. Roundy, H. Sun, M.L. Cohen, Nature **418**, 758 (2002)
52. R.S. Gonelli, A. Calzolari, D. Deghero et al., Phys. Rev. Lett. **87**, 097001 (2001)
53. J. Bardeen, L.N. Cooper, J.R. Schrieffer, Phys. Rev. **108**, 1175 (1957)
54. S.L. Bud'ko, G. Lapertot, C. Petrovic, C.E. Cunningham et al., Phy. Rev. Lett. **86**, 1877-1880 (2001)
55. P.C. Canfield, G. Crabtree, Phys. Today **56**, 34–40 (2003)
56. Y. Elstev, K. Nakao, S. Lee et al., Phys. Rev. **B 66**, 180504 (2002)
57. B. Lorenz, R.L. Meng, C.W. Chu, Phys. Rev. B **64**, 012507 (2001)
58. S. Patnaik, L.D. Cooley, A. Gurevich et al., Supercond. Sci. Technol. **14**, 315 (2001)
59. V. Braccini, A. Gurevich, J.E. Giencke et al., Phys. Rev. **B 71**, 012504 (2005)
60. Y. Kamihara, T. Watanabe, M. Hirano, H. Hosono, J. Am. Chem. Soc. **130**, 3296 (2008)
61. H. Takahashi, K. Igawa, K. Arii, Y. Kamihara, M. Hirano, H. Hosono, Nature **453**, 376 (2008)
62. J. Jaroszynski, C. Scott, F. Riggs et al., Phys. Rev. B **78**, 064511 (2008)
63. P.M. Aswathy, J.B. Anuja, P.M. Sarun, U. Syamaprasad, Supercond. Sci. Technol. **23**, 073001 (2010)
64. F. Kametani, P. Li, D. Abrrimov et al., Appl. Phys. Lett. **95**, 142502 (2009)
65. M. Rotter, M. Tegel, D. Johrendt, Phys. Rev. Lett. **101**, 107006 (2008)
66. F.C. Hsu, J.U. Luo, K.W. Yeh et al., Proc. Natl. Acad. Sci. USA **105**, 14262 (2008)
67. J. Guo, S. Jin, G. Wang et al., Phys. Rev. B **82**, 180520(R) (2010)
68. N.W. Ashcroft, Phys. Rev. Lett. **21**, 1748 (1968)
69. J.M. McMahon, M.A. Morales, C. Pierleoni, D.M. Ceperley, Rev. Mod. Phys. **84**, 1607 (2012)
70. A.P. Drozdov, M.I. Eremets, I.A. Troyan, Conventional superconductivity at 190 K at high pressures, preprint at http://arXiv.org/abs/1412.0460 (2014)
71. A.P. Drozdov, M.I. Eremets, I.A. Troyan, V. Ksenofontov, S.I. Shylin, Nature **525**, 73 (2015)
72. M. Einaga, M. Sakata, T. Ishikawa, K. Shimizu et al., Nat. Phys. **12**, 835 (2016). https://doi.org/10.1038/nphys3760
73. L.P. Gor'kov, Rev. Mod. Phys. **90**, 011001–011011 (2018)
74. F. Peng, Y. Sun, C. Pickard, R. Needs, Q. Wu, Y. Ma, Phys. Rev. Lett. **119**, 107001 (2017)
75. H. Wang, J. Tse, K. Tanaka, T. Litaka, Y. Ma, Proc. Natl. Acad. Sci. USA **109**, 6463 (2012)
76. Y. Li, J. Hao, H. Liu, J. Tse, Y. Wang, Y. Ma, Sci. Rep. **5**, 9948 (2015)
77. X. Feng, J. Zhang, G. Gao, H. Liu, H. Wang, RSC Adv. **5**, 59292 (2015)
78. A.P. Drozdov, P. P. Kong, V. S. Minkov, S. P. Besedin et al., Nature **528**, 773 (2019
79. E. Snider, N. Dasebrok, N. Dasenbrock-Gammon, R. McBride et al. Nature **586**, 377 (2020)